Article:
Cao, Zhanghua, Ji, Xiaodong, Wang, Jue et al. (4 more authors) (2022) Artificial Noise Aided Secure Communications for Cooperative NOMA Networks. IEEE Transactions on Cognitive Communications and Networking. pp. 946-963. ISSN: 2332-7731

https://doi.org/10.1109/TCCN.2021.3130979

Artificial Noise Aided Secure Communications for Cooperative NOMA Networks

Zhanghua Cao, Xiaodong Ji, *Member, IEEE,* Jue Wang, *Member, IEEE,* Wei Wang, *Member, IEEE,* Kanapathippillai Cumanan, *Senior Member, IEEE,* Zhiguo Ding, *Fellow, IEEE,* and Octavia A. Dobre, *Fellow, IEEE*

***Abstract*—Non-orthogonal multiple access (NOMA) has been envisioned as a promising multiple access technique to improve spectral efficiency and provide massive connectivity in future wireless networks. However, the inherited security issues with NOMA should be carefully addressed to further exploit its potential benefits in NOMA enabled wireless networks. As such, we consider a cooperative NOMA network, where a source uses the NOMA to simultaneously communicate with a multi-antenna near-user and a far-user. While directly communicating with the near-user, the source employs multiple full-duplex (FD) decode-and forward (DF) relays to establish communication with the far-user in the presence of a passive eavesdropper. To address the eavesdropping in this cooperative NOMA network, we propose a new two-phase FD-based artificial noise (AN) scheme with different relay selection techniques. In the first phase, the selected FD relay emits AN to confuse the eavesdropper while receiving the superimposed signal from the source. In the second phase, the selected relay performs exclusive OR (XOR) operation on both the message intended to the far-user and the AN before broadcasting the resulting mixed signal. By utilizing null-space beamforming, self-interference cancellation techniques and DF-XOR cooperative protocol, the AN in the proposed scheme can be efficiently eliminated at the near-user and far-user as well as at the selected relay. However, the AN cannot be suppressed at the eavesdropper which serves the purpose of AN through degrading the decoding capability of the eavesdropper. We evaluate the performance of the proposed scheme in terms of security-reliability trade-off (SRT). For the AN-aided scheme with max-min and partial relay selection techniques, we theoretically derive the exact and asymptotic closed-form expressions of the outage probability and intercept probability. Numerical results have been provided to validate the derivations. In addition, the results reveal that the SRT of the near-user and far-user can be improved by increasing the number of antennas at the near-user and the number of relays.**

***Index Terms*—Physical layer security, security-reliability trade-off, cognitive two-way relay networks, artificial noise, relay selection.**

This work was partially supported by the National Natural Science Foundation of China (Grant Nos. 61771263, 61771264, 61871241, 62001254), the Six Categories Talent Peak of Jiangsu Province (Grant No. KTHY-039), the Future Network Scientific Research Fund Project (Grant No. FNSRFP-2021-YB-42) and the Science and Technology Program of Nantong (Grant Nos. JC2018128, JC2019114, JC2021016, JC2021126, JC2021129). *(Corresponding author: Wei Wang.)*

Z. Cao, X. Ji and J. Wang are with School of Information Science and Technology, Nantong University, Nantong 226019, China (e-mail:cryptocaozhanghua@126.com; jxd@ntu.edu.cn; wangjue@ntu.edu.cn).

W. Wang is with the School of Information Science and Technology, Nantong University, Nantong 226019, China, and also with the Nantong Research Institute for Advanced Communication Technologies, Nantong 226019, China (e-mail:wwang2011@ntu.edu.cn).

K. Cumanan is with the Department of Electronic Engineering, University of York, York, YO10 5DD, United Kingdom (e-mail: kanapathippillai.cumanan@york.ac.uk).

Z. Ding is with the School of Electrical and Electronic Engineering, The University of Manchester, Manchester M13 9PL, United Kingdom (e-mail: zhiguo.ding@manchester.ac.uk).

O. A. Dobre is with the Faculty of Engineering and Applied Science, Memorial University, St. Johns, NL A1B 3X9, Canada (e-mail: odobre@mun.ca).

I. Introduction

With the rapid development of wireless communications techniques, there has been an explosive increase in the number of communication users and devices, and data traffic of wireless networks. For example, the Internet-of-Things (IoT) has been identified as one of the key elements to generate connected products and create services and applications that will completely rely on future wireless networks [1]. Consequently, the communication networks have been experiencing a tremendous growth in the number of devices and applications that demand access to the Internet. Moreover, the forthcoming fifth-generation (5G) and beyond networks will increase the number of connected IoT devices by many folds [2]-[4]. Thus, the data traffic in next-generation wireless networks is expected to increase explosively, and the available limited spectrum resources become more scarce. As one of the promising techniques to deal with huge demand of massive connectivity, non-orthogonal multiple access (NOMA) has been identified as an enabling technology to improve the spectral efficiency of 5G and beyond [5]-[8]. On the other hand, cooperative relaying can extend the transmission coverage and improve spectral efficiency in wireless networks [9], [10]. Thus, a combination of cooperative relaying and NOMA techniques can further improve the spectral efficiency of 5G and beyond communications systems while providing massive connectivity to support millions of devices in future wireless networks [11]-[13].

Due to the distributed architecture of next-generation wireless networks (i.e., IoT, massive machine type communications) and the broadcast nature of wireless transmission, the beyond 5G services and applications based communication networks are still vulnerable for eavesdropping attacks. Furthermore, the massive numbers of resource constrained communication users (i.e., IoT devices) make the conventional computationally expensive cryptographic encryption scheme infeasible for practical implementation in future wireless networks [14]-[18]. Since NOMA can be widely applied in next-generation wireless networks, the problem of secure communication in NOMA enabled networks needs to be investigated.

As a promising solution, physical layer security (PLS) that provides additional information-theoretic security for wiretap communication systems by exploiting physical layer dynamics of wireless channels without the distributions of secret keys, can be employed in NOMA enabled networks [19]-[20]. Furthermore, there has been a significant interest in the PLS for NOMA-based networks (i.e., [21]-[30] and [33]-[39]).

In the past few years, the PLS in one-hop wiretap NOMA networks has been studied by different research communities. For example, Ding $et\ al.$ demonstrated that the NOMA always achieves a higher secrecy unicasting rate than that of orthogonal multiple access (OMA) in a wiretap multi-user network with mixed multicasting and unicasting traffic [21]. The AN-aided beamforming and zero-forcing beamforming techniques were developed to enhance the secrecy performance for the multiple-input and single-output NOMA networks in [22] and [23], respectively. In [24] and [25], beamforming and AN were jointly used to maximize the sum secrecy rates for the multiple-input multiple-output (MIMO) NOMA networks. In [26], two transmit antenna selection schemes were proposed to safeguard the secure transmission in MIMO NOMA networks.

More recently, PLS in a wiretap cooperative NOMA network with a relay (or multiple relays) has been investigated. Specifically, the authors in [27] studied the secrecy performance of a two-user cooperative NOMA network for both amplify-and-forward (AF) and decode-and-forward (DF) relaying protocols. In [28], the cooperative NOMA scheme of [27] was further extended to a wiretap vehicular communication system, where closed-form expressions of the secrecy outage probability were derived for the half-duplex (HD) and full-duplex (FD) DF relaying strategies. Following the same framework in [27] and with an untrusted relay, the authors in [29] employed the cooperative jamming (or artificial noise (AN)) technique to avoid the eavesdropping attacks. The wiretap cooperative NOMA network in [30] is an extension of [27] and [29], where the direct links from the source to the two users were taken into account in the presence of multiple untrusted relays. Relay selection, as a promising approach to improve the PLS for the wiretap cooperative networks [31], [32], can also be adopted to improve PLS in the multi-relay wiretap cooperative NOMA networks [33]-[37]. In [33], relay selection was used to mitigate the eavesdropping attacks in a wiretap cooperative NOMA network without direct link between the source and destination nodes, for the first time. The authors of [34] proposed the two-stage and optimal relay selection schemes to enhance the PLS for the DF/AF based wiretap cooperative NOMA network. Assuming the channels in the communication system of [34] with Nakagami$-m$ fading, [35] and [36] derived the closed-form secrecy outage probability of different relay selection schemes. In [37], relay selection and AN techniques were combined to achieve confidential information transmission of the same wiretap cooperative NOMA network as in [34]. As an extension of [27] and [29], the authors in [38] and [39] studied another type of wiretap cooperative NOMA network, where the source directly transmits messages to the near-user, and communicates with the far-user via a relay. In [38], the authors utilized a multiple-antenna FD relay to implement the AN schemes to improve the secrecy performance in the considered wiretap cooperative network. The AN schemes were designed to minimize information leakage of the wiretap cooperative NOMA network with an untrusted relay in [39].

Based on the above discussions, we realize that: 1) the NOMA protocol can improve the spectral efficiency of cooperative relay networks [11]-[13], for example, it can increase the system throughput in a two users cooperative network, where a source communicates directly with the near-user, while sending messages to the far-user only through a relay (or multiple relays) [12], [40]-[41]; 2) the multi-relay aided cooperative NOMA system with a direct link between the source and the near-user can be employed in 5G and beyond wireless networks [12], [40], and UAV enabled communications [42], [43]. However, due to the broadcast nature of wireless transmissions, the considered cooperative NOMA network is vulnerable to the attacks from different eavesdroppers. Moreover, to the best of authors' knowledge, the PLS in such a wiretap cooperative NOMA network has not been considered in the literature.

Motivated by above facts, we find that it is of paramount importance to design a novel and efficient PLS communication scheme for the cooperative NOMA network, where the source can directly communicate with the multi-antenna near-user, while transmitting information to the far-user via multiple FD relays in the presence of an eavesdropper. Based on the DF-exclusive OR (DF-XOR) relaying protocol, we combine a novel AN scheme with the relay selection technique to improve the PLS performance. The XOR operation is also known as a special type of digital network coding, and has been applied in the One-Time Pad (Vernams Cipher) [44]. The source communicating with near-user and far-user consists of two phases. In the first phase, the source transmits a superimposed signal to the near-user and the selected FD relay, while the selected FD relay emits an AN to confuse the eavesdropper. In the second phase, the selected relay decodes the message for the far-user, treats the decoded message and the AN as two separated bit sequences, performs XOR operation on the obtained bit sequences, then transmits the mixture of the AN and source message to the far-user. It is worth mentioning that the AN is a secret key in the second phase.

The considered wiretap cooperative NOMA network is different from the existing cooperative NOMA systems with secrecy constraints in the literature. To be specific, on one hand, in [27]-[30] and [33]-[37], the near-user and far-user of the wiretap cooperative NOMA system are both assisted by a relay (or a set of relays), while in [38]-[39], only one relay is employed to securely establish the information exchange between the source and the far-user. This differentiates our cooperative NOMA system from the existing cooperative NOMA networks in the literature [27]-[30], [33]-[39]. To the best of our knowledge, this is the first work that adopts both the AN and relay selection techniques to enhance the secrecy performance of the wiretap multiple relays assisted NOMA network with a direct link from the source to the near-user. ***On the other hand, the AN in our secure communication scheme is not only an interfering signal to against the***

eavesdropping attacks, but also functions as a secret key to protect the confidentiality of the source message for the far-user. Thus, the proposed AN scheme is different from those of the existing schemes in the literature, where the AN is considered only as an interfering signal to confuse the eavesdroppers, i.e., [22], [24]-[25], [37]-[39] and [45]-[47]. The advantages of the proposed AN scheme are that: 1) the XOR operation prevents the eavesdropper from directly intercepting the message intended for the far-user in the second phase; 2) the AN can be reused (the same AN functions as an interfering signal and a secret key in the first and second phases, respectively).

The key contributions of this work are summarized as follow:

- For the first time in the literature, we combine the relay selection scheme with AN technique to enhance the PLS performance for the cooperative NOMA network, in which the source communicates with the far-user via a set of FD DF relays and directly transmits the intended message to the near-user. Furthermore, we design a new AN scheme, in which the AN signal offers two benefits simultaneously: an interfering signal and a secret key. However, in the existing AN schemes in the literature, i.e., [22], [24]-[25], [37]-[39] and [45]-[47], the AN functions only as an interfering signal. Thus, the proposed AN scheme differs from the existing AN schemes in the literature.
- We provide a new description of the residual self-interference (RSI) at the selected FD relay. In general, the RSI is considered as a variable with Rayleigh distribution [45] or as a constant [46]. In this paper, we assume that the RSI is an exponentially distributed random variable, when it is less than a certain threshold. Otherwise, the RSI is equal to the threshold. With these assumptions, the description of the RSI in our work becomes more accurate.
- In order to analyze the security-reliability trade-off (SRT) performance of the proposed max-min and partial (Par) relay selection schemes, we derive the closed-form expressions for the outage probability (reliability) and intercept probability (security). To further understand the insights, the asymptotic analysis of outage and intercept probabilities for the max-min and Par relay selection schemes are presented. The asymptotic performance analysis demonstrates an useful result that, even if the eavesdropper can wiretap on the data transmission for the far-user in two phases, the eavesdropper cannot obtain more meaningful information of the message for the far-user than that for the near-user in high SNR regime. Thus, the proposed AN scheme can effectively mitigate the eavesdropping attacks.

The remainder of this paper is organized as follows. The wiretap cooperative NOMA network and AN scheme are described in Section II. The secrecy performance of max-min and Par relay selection schemes are analyzed in Section III. In Section IV, numerical results are presented to validate the derived theoretical results. Finally, we conclude this paper in Section V.

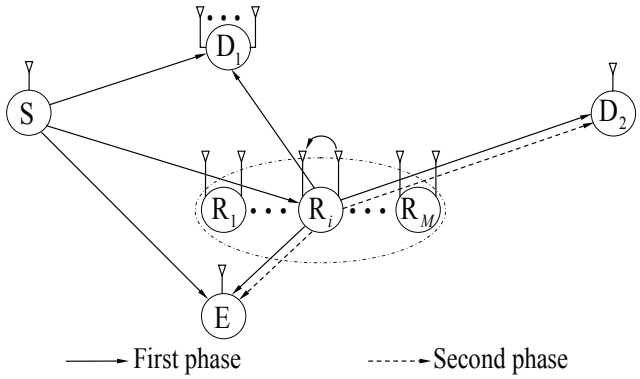

Fig. 1: A multiple full-duplex relays assisted cooperative NOMA network in the presence of an eavesdropper.

II. NOMA Enabled Cooperative Relaying Networks

A. Network Model

We consider a cooperative NOMA network, as illustrated in Fig.1, in which the source S intends to transmit messages to a near-user D_1 and a far-user D_2 in the presence of a passive eavesdropper E. In such a wiretap cooperative NOMA network, the near-user D_1 can directly communicate with the S, while the far-user D_2 uses multiple DF relays R_i ($i \in \mathcal{R} = \{1, \cdots, M\}$) to receive the corresponding message. Each relay operates in FD mode by using one transmit antenna and one receive antenna. Since the near-user D_1 demands a high data rate, we assume that D_1 is equipped with N antennas, while the source S, the far-user D_2 and the eavesdropper E have a single-antenna each. Due to severe shadowing effects caused by physical obstacles, we assume that the direct link between S and D_2 is unavailable [38], [39]. The eavesdropper might intercept the messages from the S and relays.

In the cooperative NOMA network, we assume that all the channels undergo independent and nonidentical distributed Rayleigh fading. The channel coefficients from S to R_i and E, R_i to D_2 and E are denoted by h_{si}, h_{se}, h_{id_2} and h_{ie}, respectively. It follows that the channel power gains $|h_{si}|^2, |h_{se}|^2, |h_{id_2}|^2$ and $|h_{ie}|^2$ are exponentially distributed random variables with means $\lambda_{si}, \lambda_{se}, \lambda_{id_2}$ and λ_{ie}, respectively. Let $\mathbf{h}_{sd_1}$ and $\mathbf{h}_{id_1}$ in $\mathbb{C}^{N\times 1}$ represent the channel fading vector from S to D_1 and R_i to D_1, respectively. Furthermore, the elements of $\mathbf{h}_{sd_1}$ and $\mathbf{h}_{id_1}$ are independent and identically distributed complex Gaussian random variables with zero-mean and variances λ_{sd_1} and λ_{id_1}, respectively. The channel coefficients of the same link remain constant within two phases [38], [45]. Let n_{d_2}, n_e and n_i denote the zero-mean additive white Gaussian noise (AWGN) at the receivers D_2, E and R_i, with variances $\sigma_{d_2}^2$, σ_e^2 and σ_i^2, respectively. The vector $\mathbf{n}_{d_1} \in \mathbb{C}^{N\times 1}$ is a zero-mean AWGN vector at D_1. The variance of each term in $\mathbf{n}_{d_1}$ is represented by $\sigma_{d_1}^2$.

B. Data Transmission in the First Phase

In the considered wiretap cooperative NOMA network, the FD relays are not used to improve the spectral efficiency, and instead, they are exploited to inject AN to tackle the eavesdropping attacks. Thus, the communication between S and users $\mathrm{D}_1, \mathrm{D}_2$ in this cooperative NOMA network is still accomplished in two phases, and a relay R_i is selected for this two-phase data transmissions. In the first phase, using the NOMA technique, the S adopts the superposition coding strategy, and linearly combines the signals x_1 and x_2 that are intended for D_1 and D_2, respectively. Thus, the superimposed signal can be defined as $x = \sqrt{\alpha_1}x_1 + \sqrt{\alpha_2}x_2$, where α_1 and α_2 are the power allocation coefficients for D_1 and D_2, respectively. To maintain better fairness between users, we assume that $\alpha_1 + \alpha_2 = 1$ and $\alpha_2 > \alpha_1 > 0$. Then, the source S broadcasts the superimposed signal x to D_1 and the selected relay R_i with power P_s. At the same time, the chosen relay R_i emits the AN x_J to confuse the eavesdropper E with power P_1. Similar to [48], we assume that the AN x_J is obtained by a pseudo random sequences generator. Hence, the received signals at D_1, R_i, D_2 and E can be expressed, respectively, as

$$\begin{cases} y_{sd_1} = \mathbf{w}^\dagger(\sqrt{P_s}\mathbf{h}_{sd_1}x + \sqrt{P_1}\mathbf{h}_{id_1}x_J + \mathbf{n}_{d_1}), \\ y_{si} = \sqrt{P_s}h_{si}x + \sqrt{P_1}h_{ii}x_J + n_i, \end{cases} \tag{1}$$

$$\begin{cases} y_{id_21} = \sqrt{P_1}h_{id_2}x_J + n_{d_2}, \\ y_{e1} = \sqrt{P_s}h_{se}x + \sqrt{P_1}h_{ie}x_J + n_e, \end{cases} \tag{2}$$

where $\mathbf{w}^\dagger$ is Hermitian transpose of $\mathbf{w} \in \mathbb{C}^{N\times 1}$ and satisfies $\|\mathbf{w}\|^2 = 1$ [38]. Note that x_1, x_2 and x_J are supposed to be normalized signals with unit power, i.e., $\mathbb{E}|x_1|^2 = \mathbb{E}|x_2|^2 = \mathbb{E}|x_J|^2 = 1$. Furthermore, the self-interference at R_i can be significantly suppressed, but cannot be completely eliminated. As in [45], the inevitable RSI at R_i is denoted by h_{ii} and it is assumed that $|h_{ii}|^2$ is an exponential random variable with mean λ_{ii}, which is much less than λ_{si}, i.e., $\lambda_{ii} \ll \lambda_{si}$.

According to the fundamental concepts of NOMA, the near-user D_1 first decodes x_2 by treating x_1 as an interference, and then successfully removes it by utilizing the successive interference cancellation technique. Therefore, the received signal-to-interference-plus-noise ratio (SINR) of x_2 and signal-to-noise ratio (SNR) of x_1 at D_1 are given, respectively, by

$$\Gamma_{sd_1}^{[2]} = \frac{\alpha_2 P_s|\mathbf{w}^\dagger\mathbf{h}_{sd_1}|^2}{\alpha_1 P_s|\mathbf{w}^\dagger\mathbf{h}_{sd_1}|^2 + \sigma_{d_1}^2}, \quad \Gamma_{sd_1}^{[1]} = \frac{\alpha_1 P_s|\mathbf{w}^\dagger\mathbf{h}_{sd_1}|^2}{\sigma_{d_1}^2}, \tag{3}$$

Evidently, the SINR $\Gamma_{sd_1}^{[2]}$ is an increasing function of $|\mathbf{w}^\dagger\mathbf{h}_{sd_1}|^2$. Thus, maximizing the SINR $\Gamma_{sd_1}^{[2]}$ is equivalent to maximizing $|\mathbf{w}^\dagger\mathbf{h}_{sd_1}|^2$. Similar to [38] and [47], the vector $\mathbf{w}$ is determined by solving the following optimization problem:

$$\max_{\mathbf{w}} \quad |\mathbf{w}^\dagger\mathbf{h}_{sd_1}|^2, s.t. \quad \mathbf{w}^\dagger\mathbf{h}_{id_1} = 0, \|\mathbf{w}\|^2 = 1. \tag{4}$$

Furthermore, the work in [38] and [47] presents a problem solving process and a solution for the optimization problem in (4). Using the results presented in [38] and [47], the probability density function (PDF) of $|\mathbf{w}^\dagger\mathbf{h}_{sd_1}|^2$ can be written as

$$f_{|\mathbf{w}^\dagger\mathbf{h}_{sd_1}|^2}(x) = \lambda_{sd_1}^{-(N-1)}((N-2)!)^{-1}x^{N-2}e^{-\lambda_{sd_1}^{-1}x}. \tag{5}$$

Based on (1), the SINR of x_2 at R_i can be defined as

$$\Gamma_{si}^{[2]} = \frac{\alpha_2 P_s\sigma_i^{-2}|h_{si}|^2}{\alpha_1 P_s\sigma_i^{-2}|h_{si}|^2 + P_1\sigma_i^{-2}|h_{ii}|^2 + 1}, \tag{6}$$

where $P_1\sigma_i^{-2}|h_{ii}|^2$ denotes the SNR of RSI. The PDF of $P_1\sigma_i^{-2}|h_{ii}|^2$ is $f_{P_1\sigma_i^{-2}|h_{ii}|^2}(x) = \sigma_i^2\lambda_{ii}^{-1}P_1^{-1}\ e^{-\sigma_i^2\lambda_{ii}^{-1}P_1^{-1}x}$. From a practical aspect, the RSI should be less than a given threshold [46], [49]. Therefore, the SNR of the RSI at R_i can be denoted by $\Gamma_{ii} = \min\{\frac{P_1}{\sigma_i^2}|h_{ii}|^2, \gamma_I\}$, where γ_I is the noise-normalized RSI power. Thus, the SINR at R_i can be rewritten as

$$\Gamma_{si}^{[2]} = \frac{\alpha_2 P_s\sigma_i^{-2}|h_{si}|^2}{\alpha_1 P_s\sigma_i^{-2}|h_{si}|^2 + \Gamma_{ii} + 1}, \tag{7}$$

where the cumulative distribution function (CDF) of Γ_{ii} is calculated as

$$F_{\Gamma_{ii}}(x) = \begin{cases} \frac{1-e^{-\sigma_i^2\lambda_{ii}^{-1}P_1^{-1}x}}{1-e^{-\sigma_i^2\lambda_{ii}^{-1}P_1^{-1}\gamma_I}}, & x < \gamma_I, \\ 1, & x \geqslant \gamma_I. \end{cases} \tag{8}$$

Remark 1. *In [45], the RSI was assumed to be an exponential random variable, whereas it was considered as a constant in [46], [49]. We combine these two assumptions, and assume more realistically that $\frac{P_1}{\sigma_i^2}|h_{ii}|^2$ is an exponential random variable when the RSI is less than a threshold γ_I. Otherwise, the RSI equals to γ_I. Obviously, as $\gamma_I \to \infty$, we have $\Gamma_{ii} = \frac{P_1}{\sigma_i^2}|h_{ii}|^2$. Furthermore, let $F_{\Gamma_{ii}}(x) = 0$ for $x < \gamma_I$, then we have $\Gamma_{ii} = \gamma_I$.* ***Thus, the model of the RSI in [45] or [46], [49] becomes a special case of the model considered in this work****. In addition, in the low SNR regime, modeling the RSI as an exponential random variable is more accurate than treating it as a constant. When the SNR is high, the self-interference can be significantly suppressed, and the RSI cannot be approximated as infinity, otherwise, the self-interference cancellation techniques would not offer any benefits. Therefore, the RSI is assumed to be a constant in high SNR regime. It follows that, compared to the description of RSI in existing literature (i.e., [45], [46] and [49]), the proposed characterization of the RSI is more appropriate and accurate.*

From (2), the SNR and SINR of x_J at D_2 and E can be expressed, respectively, as

$$\Gamma_{id_2J} = \frac{P_1|h_{id_2}|^2}{\sigma_{d_2}^2}, \Gamma_{ie1J} = \frac{P_1|h_{ie}|^2}{P_s|h_{se}|^2 + \sigma_e^2}. \tag{9}$$

Furthermore, similarly to [33], we also assume that the eavesdropper has high detection capacities such that the data streams received from the relay can be distinguished (i.e., we assume that the eavesdropper can detect x_1 (or x_2) without being interfered by x_2 (or x_1)). This assumption is based on the worst case scenario. As such, the SNR for detecting x_1 or x_2 at E is given by

$$\Gamma_{ie1}^{[1]} = \Gamma_{ie1}^{[2]} = \frac{P_s|h_{se}|^2}{P_1|h_{ie}|^2 + \sigma_e^2}. \tag{10}$$

C. Cooperative Relaying in the Second Phase

In the second phase, the selected relay R_i aims to decode x_2. If R_i is capable of obtaining x_2 correctly, it will combine x_2 and x_J by performing XOR operation, and then transmit $x_2 \oplus x_J$ to D_2 with power P_2. The received signals at D_2 and E can be written, respectively, as

$$\begin{cases} y_{id_2 2} = \sqrt{P_2} h_{id_2}(x_2 \oplus x_J) + n_{d_2}, \\ y_{e2} = \sqrt{P_2} h_{ie}(x_2 \oplus x_J) + n_e. \end{cases} \tag{11}$$

Accordingly, the SNR of the mixed signal $x_2 \oplus x_J$ at D_2 and E can be written as

$$\Gamma_{id_2 2} = \frac{P_2 |h_{id_2}|^2}{\sigma_{d_2}^2}, \Gamma_{ie2} = \frac{P_2 |h_{ie}|^2}{\sigma_e^2}, \tag{12}$$

respectively. In the case the selected relay R_i fails to obtain x_2, the communication between S and D_2 is considered in outage.

In the following, we provide some discussions for the considered wiretap cooperative NOMA network and the data transmissions. 1) The considered cooperative NOMA system reflects different practical scenarios, and can be deployed in the 5G and beyond wireless networks [12], [40], and in UAV relay networks [42], [43]. Specifically, in these networks, the base station (BS) can transmit messages to the cell-center user (called near-user) directly. However, due to the long distance or blockages, the BS communicates with the far-user (i.e., cell-edge user) via a ground/UAV relay node. 2) The authors in [45] revealed that the FD-aided AN techniques achieve a better secrecy performance than that of the FD relaying. Therefore, we employ the FD-aided AN techniques to improve the PLS for the proposed cooperative NOMA network. 3) In the second phase, the selected relay R_i can employ the NOMA and XOR operation to generate a signal $\overline{x} = \sqrt{\alpha_3} x_1 + \sqrt{\alpha_4}(x_2 \oplus x_J)$, where $\alpha_3 + \alpha_4 = 1$. According to the maximal ratio combining scheme, the signal $\overline{x}$ increases the SINR of x_1 at the eavesdropper. Thus, the signal $\overline{x}$ enables the eavesdropper to intercept x_1 more easily. On the other hand, in order to obtain the message x_2, the far-user should decode the signal x_J and $x_2 \oplus x_J$. However, $\overline{x}$ increases the difficulty of decoding $x_2 \oplus x_J$ from $\overline{x}$ at the far-user and leads to a decrease in the data rate between the source and the far-user. Since the data rate of the communication from S to D_1 can be increased by the multiple antenna techniques, the selected relay renounces the use of NOMA and only broadcasts the signal $x_2 \oplus x_J$ to two users. The signal $x_2 \oplus x_J$ prevents the eavesdropper from extracting useful information of messages x_1 and x_2 directly, and increases the data rate of the communication from the source to the far-user.

III. Performance Analysis of the Max-Min and Partial Relay Selection

In this section, we present the SRT performance analysis of the max-min and Par relay selection schemes by deriving exact closed-form expressions for the outage and intercept probabilities. In addition, to gain more insights into the proposed schemes, we also carry out the asymptotical analysis of the outage and intercept probabilities.

Let us first provide the definitions of the outage and intercept probabilities for the near-user D_1 and far-user D_2. Based on the NOMA principle, the near-user D_1 can successfully decode the message x_1 only if both the $\Gamma_{sd_1}^{[2]}$ and $\Gamma_{sd_1}^{[1]}$ are larger than the corresponding target transmission rates r_{o1} and r_{o2}, respectively. Thus, the outage probability of D_1 is defined as

$$P_{out1} = 1 - \Pr\left\{\Gamma_{sd_1}^{[2]} > \gamma_{o2}, \Gamma_{sd_1}^{[1]} > \gamma_{o1}\right\}, \tag{13}$$

where $\gamma_{o1} = 2^{2r_{o1}} - 1$, $\gamma_{o2} = 2^{2r_{o2}} - 1$. On the other hand, the eavesdropper E can obtain x_1 in two ways. In one way, E decodes x_1 directly, whereas the eavesdropper decodes x_J and removes it in (2) to acquire x_1 in the second way. Thus, the intercept probability of D_1 is expressed as

$$\begin{aligned} P_{int1} &= \Pr\left\{\Gamma_{ie1}^{[1]} < \gamma_{e1}, \Gamma_{ie1J} > \gamma_{e1}, \frac{P_s |h_{se}|^2}{\sigma_e^2} > \gamma_{e1}\right\} \\ &\quad + \Pr\left\{\Gamma_{ie1}^{[1]} > \gamma_{e1}\right\}, \end{aligned} \tag{14}$$

where $\gamma_{e1} = 2^{2(r_{o1} - r_{s1})} - 1$ and r_{s1} is the given secrecy rate threshold for x_1 at D_1.

The far-user D_2 can obtain x_2 only if the selected relay R_i and D_2 correctly decode x_2 and x_J, $x_2 \oplus x_J$, respectively. Due to the XOR operation, the eavesdropper E will not be able to obtain any information from $x_2 \oplus x_J$ directly [44]. However, the eavesdropper can obtain x_2 when the event $\{\Gamma_{ie1}^{[2]} > \gamma_{e2}\}$ or event $\{\Gamma_{ie1}^{[2]} < \gamma_{e2}, \Gamma_{ie1J} > \gamma_{e2}, \Gamma_{ie2} > \gamma_{e2}\}$ occurs. Thus, the outage probability and intercept probability of D_2 can be defined, respectively, as follows:

$$\begin{aligned} P_{out2} &= 1 - \Pr\left\{\Gamma_{si}^{[2]} > \gamma_{o2}, \Gamma_{id_2 J} > \gamma_{o2}, \right. \\ &\quad \left. \Gamma_{id_2 2} > \gamma_{o2}\right\}, \end{aligned} \tag{15}$$

$$\begin{aligned} P_{int2} &= \Pr\left\{\Gamma_{ie1}^{[2]} < \gamma_{e2},\ \Gamma_{ie1J} > \gamma_{e2}, \Gamma_{ie2} > \gamma_{e2}\right\} \\ &\quad + \Pr\left\{\Gamma_{ie1}^{[2]} > \gamma_{e2}\right\}, \end{aligned} \tag{16}$$

where $\gamma_{e2} = 2^{2(r_{o2} - r_{s2})} - 1$ and r_{s2} is the target secrecy rate for x_2 at D_2.

It is easy to observe that $P_{out1} = P_{out2} = 1$ as $\alpha_2 - \gamma_{o2}\alpha_1 \leqslant 0$. Thus, in the remainder of this section, we analyze the outage and intercept probabilities for the case of $\alpha_2 - \alpha_1\gamma_{o2} > 0$.

Remark 2. *Based on the definitions of the outage probabilities P_{out1} and P_{out2}, we find that $P_{out1} < 1$ and $P_{out2} < 1$ if and only if $\alpha_2 - \alpha_1\gamma_{o2} > 0$. Thus, from the mathematical perspective, the assumption $\alpha_2 > \alpha_1 > 0$ is neither sufficient nor necessary, as highlighted in [50]. However, taking into account the degraded channel conditions for the far-user and the fairness in cooperative NOMA networks, we also assume $\alpha_2 > \alpha_1 > 0$ as in [21]-[30] and [33]-[39]. Furthermore, according to the following performance analysis of the outage and intercept probabilities, we find that the outage and intercept probabilities depend on the coefficient $\frac{1}{\alpha_2 - \alpha_1\gamma_{o2}}$. Therefore, even if $\alpha_1 > \alpha_2 > 0$, the performance analysis process and closed-form expressions for the outage and intercept probabilities remain unchanged. It follows that simulation results for $\alpha_2 > \alpha_1 > 0$ are similar to those for $\alpha_1 > \alpha_2 > 0$.*

Remark 3. *Similar to [31], the outage probabilities in (13) and (15) define the failure rate of data transmission from the*

source to the NOMA users, and the intercept probabilities in (14) and (16) are the prospects for the eavesdropper to successfully decode the source messages. Thus, the lower the outage and intercept probabilities, the better the reliability and security in the considered wiretap cooperative NOMA network. In the proposed secure communication scheme, we employ the multiple antenna, relay selection and AN techniques to decrease the outage probability and intercept probability, respectively. Based on the outage and intercept probabilities, a secrecy performance metric SRT can be defined [31]. The metric SRT establishes a unified description of the relationship between the legitimate users and the eavesdropper.

A. Performance of the Max-Min Relay Selection

In practice, it is difficult to obtain the instantaneous channel state information (CSI) of wiretap links. Therefore, we combine the max-min relay selection with the proposed AN scheme to improve the PLS for the wiretap cooperative NOMA network. Max-min relay selection depends on the CSI of legitimate links and has been used previously in the literature, i.e., [37]. According to the max-min relay selection scheme, the best relay is chosen based on the following criterion:

$$i^* = \arg\max_{j\in\mathcal{R}} \min\{|h_{sj}|^2, |h_{jd_2}|^2\}. \tag{17}$$

1) Exact Performance of the Max-Min Relay Selection for D_1*:* At the near-user D_1, the closed-form expressions for outage probability and intercept probability of the max-min relay selection can be obtained through following Theorem.

Theorem 1: For the max-min relay selection scheme, the outage probability and intercept probability of the near-user D_1 *can be expressed, respectively, as*

$$\begin{aligned} P_{out1}^{\mathrm{I}} &= 1 - e^{-\lambda_{sd_1}^{-1}\max\left\{\frac{\gamma_{o1}\sigma_{d_1}^2}{\alpha_1 P_s}, \frac{\gamma_{o2}\sigma_{d_1}^2 P_s^{-1}}{\alpha_2-\alpha_1\gamma_{o2}}\right\}} \sum_{k=0}^{N-2}\frac{\lambda_{sd_1}^{-k}}{k!} \\ &\quad \times\Big[\max\Big\{\frac{\gamma_{o1}\sigma_{d_1}^2}{\alpha_1 P_s}, \frac{\gamma_{o2}\sigma_{d_1}^2 P_s^{-1}}{\alpha_2-\alpha_1\gamma_{o2}}\Big\}\Big]^k, \end{aligned} \tag{18}$$

$$P_{int1}^{\mathrm{I}} = \sum_{i=1}^{M}\sum_{l=0}^{M-1}\sum_{\mathcal{A}\subset\mathcal{R}-\{i\},|\mathcal{A}|=l}\frac{(-1)^l(Q_{1i}+Q_{2i})}{1+\sum\limits_{j\in\mathcal{A}}\frac{\lambda_{sj}^{-1}+\lambda_{jd_2}^{-1}}{\lambda_{si}^{-1}+\lambda_{id_2}^{-1}}}, \tag{19}$$

where $Q_{1i} = \frac{\lambda_{se}P_s}{\lambda_{se}P_s+\lambda_{ie}P_1\gamma_{e1}}e^{-\frac{\gamma_{e1}\sigma_e^2}{\lambda_{se}P_s}}$ *and*

$$Q_{2i} = \begin{cases} \frac{e^{-\frac{P_1\lambda_{ie}+P_s\lambda_{se}\gamma_{e1}}{P_1\lambda_{ie}P_s\lambda_{se}\gamma_{e1}^{-1}\sigma_e^{-2}}-\frac{\sigma_e^2\gamma_{e1}}{P_1\lambda_{ie}}}}{(P_1\lambda_{ie}+P_s\lambda_{se}\gamma_{e1})P_1^{-1}\lambda_{ie}^{-1}}, & (\gamma_{e1}\geqslant 1), \\ \Big[e^{-\frac{P_1\lambda_{ie}\lambda_{se}^{-1}+P_s\gamma_{e1}}{P_1\lambda_{ie}P_s\gamma_{e1}^{-1}\sigma_e^{-2}}} - e^{-\frac{(P_1\lambda_{ie}+P_s\lambda_{se}\gamma_{e1})\sigma_e^2}{P_1\lambda_{ie}P_s\lambda_{se}(\gamma_{e1}^{-1}-1)}}\Big] \\ \times\frac{P_1\lambda_{ie}}{P_1\lambda_{ie}+P_s\lambda_{se}\gamma_{e1}}e^{-\frac{\sigma_e^2\gamma_{e1}}{P_1\lambda_{ie}}} + \frac{P_1\lambda_{ie}\gamma_{e1}}{P_1\lambda_{ie}\gamma_{e1}+P_s\lambda_{se}} \\ \times e^{\frac{\sigma_e^2}{P_1\lambda_{ie}}-\frac{(P_1\lambda_{ie}\gamma_{e1}+P_s\lambda_{se})\sigma_e^2}{P_1\lambda_{ie}P_s\lambda_{se}(1-\gamma_{e1})}}, & (0<\gamma_{e1}<1), \end{cases} \tag{20}$$

and the superscript "I*" represents the max-min relay selection scheme.*

Proof: Please refer to Appendix A. □

From (3) and (13), we can see that the derivation of outage probability mainly involves the CSI of links from S to D_1. However, the max-min relay selection scheme depends on the CSI of links $\mathrm{S}\to\mathrm{R}_i$ and $\mathrm{R}_i\to\mathrm{D}_2$. Thus, the outage probability at D_1 is not affected by the max-min relay selection scheme, which can be seen from the derivation of P_{out1}^{I} in Appendix A.

2) Asymptotic Performance of the Max-Min Relay Selection for D_1*:* In order to gain more insights into the max-min scheme of D_1, an asymptotic study is carried out in the high SNR regime. The following theorem provides the closed-form approximations for P_{out1}^{I} and P_{int1}^{I}.

Theorem 2: The outage probability P_{out1}^{I} *and intercept probability* P_{int1}^{I} *can be approximated as follows:*

$$P_{out1}^{\mathrm{I}} \approx [(N-1)!]^{-1}(\sigma_{d_1}^2\gamma_{o1}(\lambda_{sd_1}P_s\alpha_1)^{-1})^{N-1}, \tag{21}$$

$$\begin{aligned} P_{int1}^{\mathrm{I}} &\approx \sum_{i=1}^{M}\frac{\beta_1^M}{M}\Big[\frac{P_1\lambda_{ie}\min\{\gamma_{e2},\gamma_{e2}^{-1}\}}{P_1\lambda_{ie}\min\{\gamma_{e2},\gamma_{e2}^{-1}\}+P_s\lambda_{se}} \\ &\quad +\frac{P_s\lambda_{se}}{P_s\lambda_{se}+P_1\lambda_{ie}\gamma_{e2}}\Big]\Big[\prod_{j\in\mathcal{R}}(\frac{1}{\lambda_{sj}}+\frac{1}{\lambda_{jd_2}})\Big] \end{aligned} \tag{22}$$

Proof: Please refer to Appendix B. □

3) Exact Performance of the Max-Min Relay Selection for D_2*:* For the far-user D_2, the following theorem provides the expressions for the outage and intercept probabilities of max-min relay selection scheme.

Theorem 3: Let $\theta_0 = \gamma_{o2}\max\{\sigma_{d_2}^2P_1^{-1}, \sigma_{d_2}^2P_2^{-1}\}, \theta_{1i} = \gamma_{o2\sigma_i^2}(\alpha_2-\alpha_1\gamma_{o2})^{-1}P_s^{-1}$*. When* $\theta_0\leqslant\theta_{1i}$*, the outage probability and intercept probability of the max-min relay selection scheme for the far-user* D_2 *can be written, respectively, as*

$$P_{out2}^{\mathrm{I}} = 1 - \sum_{i=1}^{M}(P_{1i}+P_{2i}), \tag{23}$$

$$P_{int2}^{\mathrm{I}} = \sum_{i=1}^{M}\sum_{l=0}^{M-1}\sum_{\mathcal{A}\subset\mathcal{R}-\{i\},|\mathcal{A}|=l}\frac{(-1)^l(Q_{3i}+Q_{4i})}{1+\sum\limits_{j\in\mathcal{A}}\frac{\lambda_{sj}^{-1}+\lambda_{jd_2}^{-1}}{\lambda_{si}^{-1}+\lambda_{id_2}^{-1}}}, \tag{24}$$

where the closed-form expressions of P_{1i} *and* P_{2i} *are given, respectively, by (25) and (26), and* $Q_{3i} = \frac{P_s\lambda_{se}}{(P_s\lambda_{se}+P_1\lambda_{ie}\gamma_{e2})}e^{-\frac{\gamma_{e2}\sigma_e^2}{P_s\lambda_{se}}}$*. The* Q_{4i} *in (24) is written as*

$$Q_{4i} = \begin{cases} e^{-\frac{\gamma_{e2}}{\lambda_{ie}}\max\left\{\frac{\sigma_e^2}{P_1},\frac{\sigma_e^2}{P_2}\right\}} - \frac{P_s\lambda_{se}\gamma_{e2}e^{\frac{\sigma_e^2}{P_s\lambda_{se}}}}{P_1\lambda_{ie}+P_s\lambda_{se}\gamma_{e2}} \\ e^{-\left(\frac{\gamma_{e2}}{\lambda_{ie}}+\frac{P_1}{P_s\lambda_{se}}\right)\max\left\{\frac{\sigma_e^2}{P_1},\frac{\sigma_e^2}{P_2}\right\}}, & (\gamma_{e1}\geqslant 1), \\ \varphi_{1i}+\varphi_{2i}, & (0<\gamma_{e1}<1), \end{cases} \tag{27}$$

where

$$\begin{aligned} \varphi_{1i} &= e^{-\frac{\gamma_{e2}}{\lambda_{ie}}\max\left\{\frac{\sigma_e^2}{P_2},\frac{\sigma_e^2}{P_1(1-\gamma_{e2})}\right\}-\frac{\sigma_e^2\gamma_{e2}}{P_s\lambda_{se}(1-\gamma_{e2})}} \\ &\quad -\frac{e^{-\frac{\sigma_e^2\gamma_{e2}}{P_s\lambda_{se}}-(\frac{\gamma_{e2}}{\lambda_{ie}}+\frac{P_1\gamma_{e2}^2}{P_s\lambda_{se}})\max\left\{\frac{\sigma_e^2}{P_2},\frac{\sigma_e^2}{P_1(1-\gamma_{e2})}\right\}}}{(P_s\lambda_{se}+\gamma_{e2}P_1\lambda_{ie})P_s^{-1}\lambda_{se}^{-1}}. \end{aligned} \tag{28}$$

$$P_{1i} = \sum_{i=1}^{M}\sum_{l=0}^{M-1}\sum_{\mathcal{A}\subset\mathcal{R}-\{i\},|\mathcal{A}|=l}\frac{(-1)^l}{\lambda_{id_2}}\Big\{\Big[\frac{e^{-\theta_{1i}\delta_{1i\mathcal{A}}}-e^{-(\gamma_I+1)\theta_{1i}\delta_{1i\mathcal{A}}}}{\delta_{1i\mathcal{A}}}-\frac{P_1\lambda_{ii}\theta_{1i}(e^{-\theta_{1i}\delta_{2i\mathcal{A}}}-e^{-(\gamma_I+1)\theta_{1i}\delta_{2i\mathcal{A}}})}{\delta_{2i\mathcal{A}}(\lambda_{si}\sigma_i^2+P_1\lambda_{ii}\theta_{1i})}e^{\frac{\sigma_i^2}{P_1\lambda_{ii}}}\Big]$$
$$\times\big(1-e^{-\frac{\sigma_i^2\gamma_I}{P_1\lambda_{ii}}}\big)^{-1}+\frac{\eta_{1i}}{\delta_{3i\mathcal{A}}}\big(e^{-\theta_0\delta_{3i\mathcal{A}}}-e^{-\theta_{1i}\delta_{3i\mathcal{A}}}\big)+\frac{e^{-(\gamma_I+1)\theta_{1i}\delta_{1i\mathcal{A}}}}{\delta_{1i\mathcal{A}}}+\frac{\eta_{2i}}{\delta_{3i\mathcal{A}}}\big(e^{-\theta_0\delta_{3i\mathcal{A}}}-e^{-(\gamma_I+1)\theta_{1i}\delta_{3i\mathcal{A}}}\big)\Big\}. \quad (25)$$

$$P_{2i} = \sum_{i=1}^{M}\sum_{l=0}^{M-1}\sum_{\mathcal{A}\subset\mathcal{R}-\{i\},|\mathcal{A}|=l}\frac{(-1)^l}{\lambda_{si}}\Big\{\Big[\eta_{3i}\big(e^{-\frac{\theta_{1i}}{\lambda_{id_2}}}-e^{-(\gamma_I+1)\frac{\theta_{1i}}{\lambda_{id_2}}}\big)-\frac{(e^{-\theta_{1i}\delta_{1i\mathcal{A}}}-e^{-(\gamma_I+1)\theta_{1i}\delta_{1i\mathcal{A}}})}{\delta_{1i\mathcal{A}}(\delta_{1i\mathcal{A}}\lambda_{id_2}-1)}$$
$$+\frac{(e^{-\theta_{1i}\delta_{2i\mathcal{A}}}-e^{-(\gamma_I+1)\theta_{1i}\delta_{2i\mathcal{A}}})}{\delta_{2i\mathcal{A}}(\delta_{2i\mathcal{A}}\lambda_{id_2}-1)}e^{\frac{\sigma_i^2}{P_1\lambda_{ii}}}\Big]\big(1-e^{-\frac{\sigma_i^2\gamma_I}{P_1\lambda_{ii}}}\big)^{-1}+\eta_{4i}e^{-\frac{(\gamma_I+1)\theta_{1i}}{\lambda_{id_2}}}-\frac{e^{-(\gamma_I+1)\theta_{1i}\delta_{1i\mathcal{A}}}}{\delta_{1i\mathcal{A}}(\delta_{1i\mathcal{A}}\lambda_{id_2}-1)}\Big\}. \quad (26)$$

$$\varphi_{2i}=\begin{cases}e^{-\frac{\gamma_{e2}}{\lambda_{ie}}\max\left\{\frac{\sigma_e^2}{P_1},\frac{\sigma_e^2}{P_2}\right\}}-e^{-\frac{\sigma_e^2\gamma_{e2}}{P_1(1-\gamma_{e2})\lambda_{ie}}}\\ -\frac{P_s\lambda_{se}\gamma_{e2}e^{\frac{\sigma_e^2}{P_s\lambda_{se}}}}{P_s\lambda_{se}\gamma_{e2}+P_1\lambda_{ie}}\Big[e^{-(\frac{\gamma_{e2}}{\lambda_{ie}}+\frac{P_1}{\lambda_{se}P_s})\max\left\{\frac{\sigma_e^2}{P_1},\frac{\sigma_e^2}{P_2}\right\}}\\ -e^{-(\frac{\gamma_{e2}}{\lambda_{ie}}+\frac{P_1}{\lambda_{se}P_s})\frac{\sigma_e^2}{P_1(1-\gamma_{e2})}}\Big]+\big(1-e^{-\frac{\sigma_e^2\gamma_{e2}}{P_s\lambda_{se}(1-\gamma_{e2})}}\big)\\ e^{-\frac{\sigma_e^2\gamma_{e2}}{P_1\lambda_{ie}(1-\gamma_{e2})}}, \qquad (\frac{\sigma_e^2\gamma_{e2}}{P_2}<\frac{\sigma_e^2\gamma_{e2}}{P_1(1-\gamma_{e2})}),\\ \big(1-e^{-\frac{\sigma_e^2\gamma_{e2}}{P_s\lambda_{se}(1-\gamma_{e2})}}\big)e^{-\frac{\sigma_e^2\gamma_{e2}}{P_2\lambda_{ie}}}, (\frac{\sigma_e^2\gamma_{e2}}{P_2}\geqslant\frac{\sigma_e^2\gamma_{e2}}{P_1(1-\gamma_{e2})}).\end{cases} \quad (29)$$

Proof: Please refer to Appendix C. □

In the case of $\theta_0 > \theta_{1i}$, the closed-form expression of P_{out2}^{I} can be derived by using the same mathematical techniques in the proof of Theorem 3.

4) Asymptotic Performance of the Max-Min Relay Selection for D_2*:* In this subsection, we analyze the asymptotic performance of the max-min relay selection scheme for D_2, and provide the approximations of P_{out2}^{I} and P_{int2}^{I} in the following theorem.

Theorem 4: The outage probability P_{out2}^{I} and intercept probability P_{int2}^{I} of the max-min relay selection scheme for the far-user D_2 are approximated as

$$P_{out2}^{\mathrm{I}} \approx \xi_M\prod_{i\in\mathcal{R}}\Big[\frac{\gamma_I+1}{\lambda_{si}\theta_{1i}^{-1}}+\frac{\max\{P_1^{-1},P_2^{-1}\}}{\lambda_{id_2}\gamma_{o2}^{-1}\sigma_{d_2}^{-2}}\Big], \quad (30)$$

$$P_{int2}^{\mathrm{I}} \approx \sum_{i=1}^{M}\frac{\beta_1^M}{M}\Big[\frac{P_1\lambda_{ie}\min\{\gamma_{e2},\gamma_{e2}^{-1}\}}{P_1\lambda_{ie}\min\{\gamma_{e2},\gamma_{e2}^{-1}\}+P_s\lambda_{se}}+\frac{P_s\lambda_{se}}{P_s\lambda_{se}+P_1\lambda_{ie}\gamma_{e2}}\Big]\Big[\prod_{j\in\mathcal{R}}(\frac{1}{\lambda_{sj}}+\frac{1}{\lambda_{jd_2}})\Big] \quad (31)$$

where the coefficient ξ_M is obtained by the Monte-Carlo method.

Proof: Please refer to Appendix D. □

In the considered cooperative NOMA network, the eavesdropper can intercept x_1 in the first phase, whereas the transmission of message x_2 includes two phases and the eavesdropper intends to intercept information of x_2 in the first and second phases. However, from Theorem 2 and Theorem 4, we can observe that the approximations of P_{int1}^{I} and P_{int2}^{I} are the same for the max-min relay selection in high SNR regime. This observation reveals an interesting result that, although the eavesdropper can respectively wiretap on the data transmission of x_1 and x_2 in the first and the two phases, the eavesdropper cannot intercept more information of x_2 than that of x_1 in high SNR regime. This indicates that the proposed AN scheme for the considered cooperative NOMA network can effectively prevent the eavesdropper from extracting more meaningful information about x_2 of the obtained signals.

B. Performance Analysis of the Par Relay Selection

The Par relay selection assumes that only the instantaneous CSI of links $\mathrm{S}\to\mathrm{R}_i$ ($i\in\mathcal{R}$) is available. In particular, the Par scheme chooses the relay that has the best channel gain of links $\mathrm{S}\to\mathrm{R}_i$ ($i\in\mathcal{R}$). Thus, the following criterion is chosen for the Par relay selection:

$$i^* = \arg\max_{j\in\mathcal{R}}|h_{sj}|^2. \quad (32)$$

1) Exact Performance of the Par Relay Selection for D_1*:* We can obtain the outage and intercept probabilities of the Par scheme for D_1 by following steps that are similar to those in the proof for Theorem 1.

Theorem 5: The outage probability P_{out1}^{II} and intercept probability P_{int1}^{II} of the near-user D_1 with the Par scheme can be written, respectively, as

$$P_{out1}^{\mathrm{II}} = P_{out1}^{\mathrm{I}}, \quad (33)$$

$$P_{int1}^{\mathrm{II}} = \sum_{i=1}^{M}\sum_{l=0}^{M-1}\sum_{\mathcal{A}\subset\mathcal{R}-\{i\},|\mathcal{A}|=l}\frac{(-1)^l(Q_{1i}+Q_{2i})}{1+\lambda_{si}\sum\limits_{j\in\mathcal{A}}\lambda_{sj}^{-1}}, \quad (34)$$

where the superscript "II*" represents the Par relay selection scheme.*

Proof: As in Appendix A, we have $P_{out1}^{\mathrm{II}} = P_{out1}^{\mathrm{I}}$. In addition, the intercept probability P_{int1}^{II} can be defined as $P_{int1}^{\mathrm{II}} = \sum\limits_{i=1}^{M}(Q_{1i}+Q_{2i})\Pr\{T_i < |h_{si}|^2\}$, where $T_i = \max\limits_{j\in\mathcal{R}-\{i\}}|h_{sj}|^2$. Similar to the derivation of (A.5), we can calculate $\Pr\{T_i<|h_{si}|^2\}$ as

$$\Pr\{T_i<|h_{si}|^2\} = \int_0^\infty\Pr\{T_i<x\}f_{|h_{si}|^2}(x)dx = \sum_{l=0}^{M-1}\sum_{\mathcal{A}\subset\mathcal{R}-\{i\},|\mathcal{A}|=l}\frac{(-1)^l}{1+\sum\limits_{j\in\mathcal{A}}\frac{\lambda_{si}}{\lambda_{sj}}} \quad (35)$$

The intercept probability P_{int1}^{II} can be derived by replacing

$\Pr\{Z_i < \min\{|h_{si}|^2, |h_{id_2}|^2\}\}$ with (35) in (A.2). □

According to Theorem 1 and Theorem 5, for the near-user D_1, the outage probability of max-min scheme is equal to that of the Par scheme. In addition, the expression of P_{int1}^{I} is similar to P_{int1}^{II}. Furthermore, it can be easily seen that $P_{int1}^{\mathrm{I}} = P_{int1}^{\mathrm{II}}$ when $\lambda_{si} = \lambda_{id_2}$ $(i \in \mathcal{R})$. Thus, for the near-user D_1, the max-min and Par relay selection schemes get similar SRT performance, which is validated by the numerical results.

2) Asymptotic Performance of the Par Relay Selection for D_1*:* By using the same techniques as outlined in the derivation of (B.3), we can approximate $\Pr\left\{T_i < |h_{si}|^2\right\}$ as $\Pr\left\{T_i < |h_{si}|^2\right\} \approx \frac{1}{M}\big[\prod_{j\in\mathcal{R}} \frac{1}{\lambda_{sj}}\big]\beta_2^M$, where $\beta_2 = \min_{j\in\mathcal{R}} \lambda_{sj}$. Hence, we can derive the following theorem directly.

Theorem 6: The approximations of P_{out1}^{II} *and* P_{int1}^{II} *are given, respectively, by*

$$P_{out1}^{\mathrm{II}} \approx [(N-1)!]^{-1}[\sigma_{d_1}^2\gamma_{o1}(\lambda_{sd_1}P_s\alpha_1)^{-1}]^{N-1}, \quad (36)$$

$$P_{int1}^{\mathrm{II}} \approx \sum_{i=1}^{M} \frac{\beta_2^M}{M}\Big[\frac{P_1\lambda_{ie}\min\{\gamma_{e2}, \gamma_{e2}^{-1}\}}{P_1\lambda_{ie}\min\{\gamma_{e2}, \gamma_{e2}^{-1}\} + P_s\lambda_{se}} + \frac{P_s\lambda_{se}}{P_s\lambda_{se} + P_1\lambda_{ie}\gamma_{e2}}\Big]\Big[\prod_{j\in\mathcal{R}} \frac{1}{\lambda_{sj}}\Big]. \quad (37)$$

3) Exact Performance of the Par Relay Selection for D_2*:* This subsection provides the derivations of the outage and intercept probabilities of the Par scheme for D_2.

Theorem 7: For the far-user D_2*, the outage probability of the Par scheme is given by (38), and the intercept probability of the Par scheme is expressed as*

$$P_{int2}^{\mathrm{II}} = \sum_{i=1}^{M}\sum_{l=0}^{M-1}\sum_{\mathcal{A}\subset\mathcal{R}-\{i\},|\mathcal{A}|=l} \frac{(-1)^l(Q_{3i}+Q_{4i})}{1+\lambda_{si}\sum_{j\in\mathcal{A}}\lambda_{sj}^{-1}}, \quad (39)$$

where the closed-from expressions of Q_{3i} *and* Q_{4i} *are given in Theorem 3.*

Proof: Using (15) and the total probability formula [31], [32], we can formulate P_{out2}^{II} as

$$P_{out2}^{\mathrm{II}} = 1 - \sum_{i=1}^{M} \underbrace{\Pr\Big\{|h_{id_2}|^2 > \gamma_{o2}\max\{\frac{\sigma_{d_2}^2}{P_1}, \frac{\sigma_{d_2}^2}{P_2}\}\Big\}}_{P_{3i}} \underbrace{\Pr\{\Gamma_{si}^{[2]} > \gamma_{o2}, |h_{si}|^2 > T_i\}}_{P_{4i}}. \quad (40)$$

Since $|h_{id_2}|^2$ is an exponential random variable, we have $P_{3i} = e^{-\lambda_{id_2}^{-1}\gamma_{o2}\max\{\sigma_{d_2}^2P_1^{-1}, \sigma_{d_2}^2P_2^{-1}\}}$. By using (8) and adopting the same steps as in the derivation of P_{1i} and P_{2i}, the P_{4i} can be defined as

$$P_{4i} = \int_{\theta_{1i}}^{(\gamma_I+1)\theta_{1i}} \frac{\Pr\{T_i < x\}f_{|h_{si}|^2}(x)dx}{\Pr\{\Gamma_{ii} < \theta_{1i}^{-1}x - 1\}^{-1}} + \int_{(\gamma_I+1)\theta_{1i}}^{\infty} \Pr\{T_i < x\}f_{|h_{si}|^2}(x)dx. \quad (41)$$

By performing simple mathematical manipulations, we can solve the integral in (41) and obtain P_{4i}. Then, substituting P_{3i} and P_{4i} into (40), we can derive the closed-form expression of the outage probability P_{out2}^{II} as (38), where $\delta_{4i\mathcal{A}} = \lambda_{si}^{-1} + \sum_{j\in\mathcal{A}}\lambda_{sj}^{-1}$.

Following steps that are similar to those in the proof for Theorem 3, the closed-form expression of P_{int2}^{II} can be derived. □

4) Asymptotic Performance of the Par Relay Selection for D_2*:* To obtain insightful analytical results, an asymptotic study of P_{out2}^{II} and P_{int2}^{II} is carried out in high SNR regime. The outage probability P_{out2}^{II} and intercept probability P_{int2}^{II} are approximated as in the following theorem.

Theorem 8: The asymptotic expressions of P_{out2}^{II} *and* P_{int2}^{II} *are given, respectively, by*

$$P_{out2}^{\mathrm{II}} \approx \gamma_{o2}\sigma_{d_2}^2\lambda_{i^*d_2}^{-1}\max\{P_1^{-1}, P_2^{-1}\} + \prod_{i\in\mathcal{R}}\theta_{1i^*}(\gamma_I+1)\lambda_{si}^{-1}, \quad (42)$$

$$P_{int2}^{\mathrm{II}} \approx \sum_{i=1}^{M}\Big[\frac{P_1\lambda_{ie}\min\{\gamma_{e2}, \gamma_{e2}^{-1}\}}{P_1\lambda_{ie}\min\{\gamma_{e2}, \gamma_{e2}^{-1}\} + P_s\lambda_{se}} + \frac{P_s\lambda_{se}}{P_s\lambda_{se} + P_1\lambda_{ie}\gamma_{e2}}\Big]\frac{\beta_2^M}{M}\Big[\prod_{j\in\mathcal{R}}\frac{1}{\lambda_{sj}}\Big]. \quad (43)$$

Proof: From (15), the outage probability of the Par scheme for D_2 can be defined as

$$P_{out2}^{\mathrm{II}} = 1 - \Pr\{|h_{i^*d_2}|^2 > \gamma_{o2}\sigma_{d_2}^2\max\{P_1^{-1}, P_2^{-1}\}\} \times \Pr\{|h_{si^*}|^2 > (\gamma_I+1)\theta_{1i^*}\} = 1 - (1 - e^{-\lambda_{i^*d_2}^{-1}\gamma_{o2}\sigma_{d_2}^2\max\{P_1^{-1}, P_2^{-1}\}}) \times \Big[1 - \prod_{i\in\mathcal{R}}\big(1 - e^{-\lambda_{si}^{-1}\theta_{1i^*}(\gamma_I+1)}\big)\Big]. \quad (44)$$

Substituting the limits $\lim_{\min\{P_1,P_2\}\to\infty} e^{-\max\{\frac{1}{P_1}, \frac{1}{P_2}\}\lambda_{i^*d_2}^{-1}\gamma_{o2}\sigma_{d_2}^2} = 1 - \max\{\frac{1}{P_1}, \frac{1}{P_2}\}\lambda_{i^*d_2}^{-1}\gamma_{o2}\sigma_{d_2}^2$ and $\lim_{P_s\to\infty} e^{-\lambda_{si}^{-1}\theta_{1i^*}(\gamma_I+1)} = 1 - \lambda_{si}^{-1}\theta_{1i^*}(\gamma_I+1)$ into (44), we can directly express the approximation of P_{out2}^{II} as (42).

Similar to Theorem 4, we can write the approximation of P_{int2}^{II} as (43). □

Based on the derived approximations of P_{out2}^{I} and P_{out2}^{II} in Theorem 4 and Theorem 8, we can conclude that the diversity order of the max-min and Par schemes are M and 1, respectively, as the transmit SNR$\to\infty$. Thus, the outage probability of the max-min scheme is much less than that of the Par scheme in high SNR regime. On the other hand, the proposed relay selection schemes depend on the CSI h_{si} and h_{id_2}, whereas the intercept probability is determined by the CSI of the wiretap links. It follows that the intercept probability for the far-user D_2 is not influenced by the proposed relay selection schemes. Therefore, the SRT performance of the max-min scheme is much better than that of the Par scheme. Moreover, the numerical results in Section IV further confirm these observations. In addition, the formulas (37) and (43) demonstrate that the asymptotic intercept probability of P_{int1}^{II} is equal to that of P_{int2}^{II}. Therefore, for the Par relay selection, the eavesdropper still cannot obtain more useful information of x_2 than that of x_1 in high SNR regime.

$$P_{out2}^{\mathrm{II}} = 1-\sum_{i=1}^{M}\sum_{l=0}^{M-1}\sum_{\mathcal{A}\subset\mathcal{R}-\{i\},|\mathcal{A}|=l}\frac{(-1)^l}{\lambda_{si}}\Big\{\big(1-e^{-\frac{\sigma_i^2\gamma_I}{P_1\lambda_{ii}}}\big)^{-1}\Big[\frac{1}{\delta_{4i\mathcal{A}}}\big(e^{-\theta_{1i}\delta_{4i\mathcal{A}}}-e^{-(\gamma_I+1)\theta_{1i}\delta_{4i\mathcal{A}}}\big) - \frac{P_1\lambda_{ii}\theta_{1i}}{\sigma_i^2+P_1\lambda_{ii}\theta_{1i}\delta_{4i\mathcal{A}}}\big(e^{-\theta_{1i}\delta_{4i\mathcal{A}}}-e^{-\frac{\sigma_i^2\gamma_I}{P_1\lambda_{ii}}-(\gamma_I+1)\theta_{1i}}\big)\Big]+\frac{1}{\delta_{4i\mathcal{A}}}e^{-\theta_{1i}\delta_{4i\mathcal{A}}(\gamma_I+1)}\Big\}e^{-\frac{\gamma_{o2}\sigma_{d_2}^2}{\lambda_{id_2}}\max\{P_1^{-1},P_2^{-1}\}}. \quad (38)$$

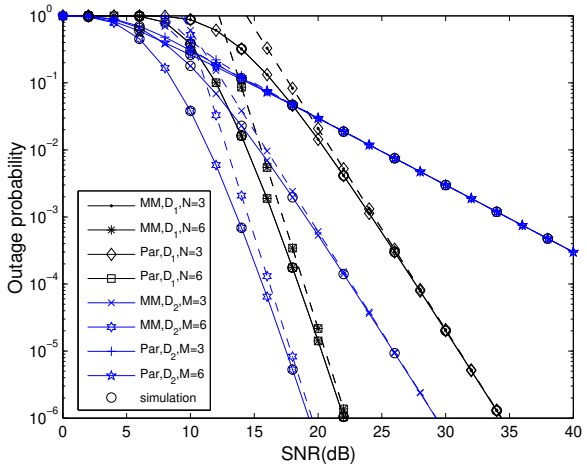

Fig. 2: The outage probability versus SNR of the max-min and Par relay selection schemes for D_1 and D_2 with $\gamma_{o1}=5$ and $\gamma_{o2}=3$. The dashed lines represent the asymptotic outage probability.

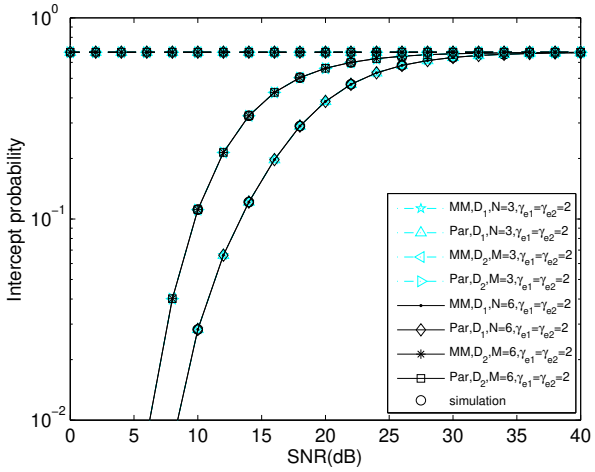

Fig. 3: The intercept probability versus SNR of max-min and Par relay selection schemes for D_1 and D_2 with $N=M=3,6$ and $\gamma_{e1}=\gamma_{e2}=2$. The dashed lines represent the asymptotic intercept probability.

IV. Numerical Results

In this section, Monte Carlo simulation-based numerical results are provided to verify the accuracy of the analytical expressions derived in Sections III. Without loss of generality, we assume that the wiretap cooperative NOMA network in Section II is generated in a two dimensional plane, where the source S, near-user D_1, far-user D_2, eavesdropper E and R_i $(i\in\mathcal{R})$ are located at coordinates of $(-1,0)$, $(-0.5,0.866)$, $(1,0)$, $(0,-2)$ and $(0.1\cos\frac{2\pi i}{M},0.1\sin\frac{2\pi i}{M})$, respectively. Furthermore, we assume that all channel coefficients are generated based on Rayleigh block fading with the path-loss exponent $\beta=3$. Thus, the average channel gain between two nodes can be defined as $d^{-\beta}$, where d denotes the Euclidean distance. For illustration purpose, we set the transmit power and noise variance as $P_s=P_1=P_2=P$ and $\sigma_i^2=\sigma_{d_1}^2=\sigma_{d_2}^2=\sigma_e^2=\sigma^2$, respectively. Therefore, the transmit SNR can be denoted as $\frac{P}{\sigma^2}$. Additionally, the RSI power threshold γ_I, the ratio $\eta=\frac{\lambda_{ii}}{\lambda_{si}}$, and the power allocation coefficient α_1 are set to $\gamma_I=1$, $\eta=0.02$ and $\alpha_1=0.1$, unless otherwise stated. In the following Figs. 2-8, it can be seen that the exact analytical curves of the outage probability, intercept probability and SRT for D_1 and D_2 are the same as the corresponding simulation results, which validates the correctness of our theoretical derivations and analytical results.

Fig. 2 illustrates the outage probability performance of the max-min and Par relay selection schemes for D_1 and D_2 with $N=3,6$, $M=3,6$, $\gamma_{o1}=5$ and $\gamma_{o2}=3$. In this figure,

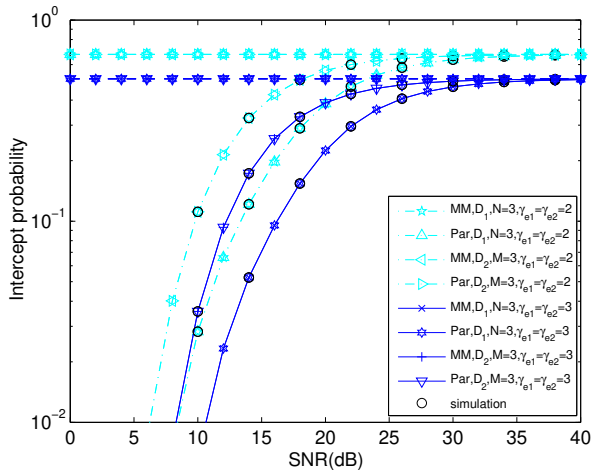

Fig. 4: The intercept probability versus SNR of max-min and Par relay selection schemes for D_1 and D_2 with $N=M=3$ and $\gamma_{e1}=\gamma_{e2}=2,3$. The dashed lines represent the asymptotic intercept probability.

we can first observe that the outage probability of D_1 and D_2 is improved by increasing the number of antennas and the number of relays, respectively. Moreover, for the far-user D_2, the improvement of the outage probability of the max-min scheme is much more obvious than that of the Par scheme. This is due to the fact that the Par scheme does not take into

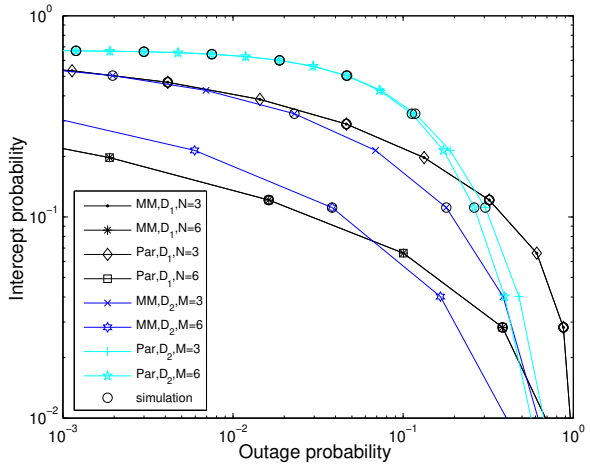

Fig. 5: Intercept probability versus outage probability of the max-min and Par relay selection schemes for different N and M with $\gamma_{o1} = 5$, $\gamma_{o2} = 3$ and $\gamma_{e1} = \gamma_{e2} = 2$.

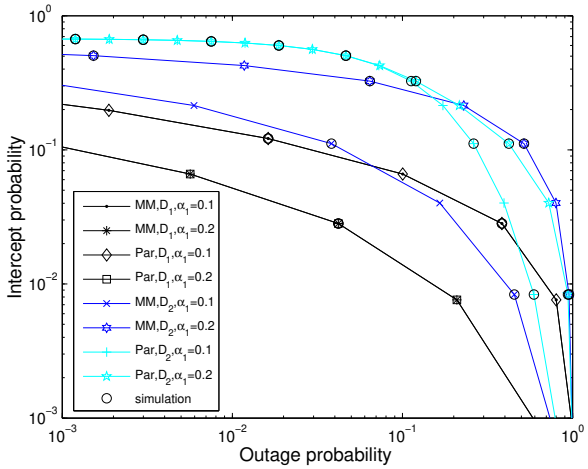

Fig. 6: Intercept probability versus outage probability of the max-min and Par relay selection schemes for different power allocation coefficients α_1 and α_2 with $N = 6$, $M = 6$, $\gamma_{o1} = 5$, $\gamma_{o2} = 3$ and $\gamma_{e1} = \gamma_{e2} = 2$.

consideration the CSI of the legitimate links in the second phase. For the same reason, we can observe from Fig. 2 that, for the far-user D_2, the outage probability of the max-min scheme is much better than that of the Par scheme. However, with the same number of antennas, the outage probability of the max-min scheme for the near-user D_1 is equal to that of the Par scheme, which means that the outage probability of D_1 is not affected by the proposed relay selection schemes. This is because the proposed relay selection schemes are obtained by utilizing the CSI of links $\mathrm{S} \to \mathrm{R}_i$ and $\mathrm{R}_i \to \mathrm{D}_2$, while the outage probability of D_1 is determined by the channel fading vector $\mathbf{h}_{sd_1}$. Furthermore, the curves of asymptotic outage probability of the max-min and Par schemes can be evaluated by analytical expressions provided in Sections III. Similar to [52]-[54], adopting the Monte-Carlo method with SNR=40 dB to generate the numerical results of (46), we can derive the coefficients $\xi_3 = 1.18591$ and $\xi_6 = 1.99058$. Finally, we can also observe that, the asymptotic curves of the outage probability for the max-min and Par schemes approach the exact ones at high SNR, which confirms the accuracy of our asymptotic analysis.

Figs. 3 and 4 present the intercept probability versus SNR for the proposed relay selection schemes. From Fig. 3, it can be seen that the intercept probability of the data transmissions between S and D_1, D_2 is not affected by N, M and the proposed relay selection schemes. This is consistent with the fact that the max-min and Par schemes depend on the CSI of legitimate links, while the intercept probability is determined by the SNR/SINR of the wiretap channels. Fig. 4 depicts that the intercept probability of each relay selection scheme for D_1, D_2 decreases as $\gamma_{e1} = \gamma_{e2}$ increases from 2 to 3. Additionally, as can be seen in Fig. 4, the intercept probability of D_1 is almost equal to that of D_2 in high SNR regime. In this case, the eavesdropper cannot extract more information of signal x_2 than that of x_1. It follows that the proposed DF-XOR relaying protocol for the data transmission between S and D_2 can effectively deal with the eavesdropping attacks.

From Figs. 2, 3 and 4, it can be seen that the outage probability and intercept probability are decreasing and increasing functions of SNR, respectively. Taking into account the discussions of Remark 3, we can obtain a conclusion that there exists a trade-off between the security (intercept probability) and reliability (outage probability) of the proposed secure communication scheme. The performance metric of security-reliability trad-off is abbreviated as SRT. In the following Figs. 5-8, we can observe that, for each SRT curve, the outage/intercept probability decreases as the intercept/outage probability increases. Fig. 5 illustrates the impact of N and M on the SRT performance of the proposed relay selection schemes for D_1 and D_2, respectively. As expected, it is clearly shown that increasing N and M can respectively enhance the SRT of the max-min/Par scheme for D_1 and D_2. Furthermore, for the data transmission from S to D_2, as the number of relays increases, the improvement of SRT for the max-min scheme is much higher than that for the Par scheme. This trend is due to the fact that the SRT of the Par scheme is limited by the CSI of $\mathrm{R}_i \to \mathrm{D}_2 (i \in \mathcal{R})$ links. In Fig. 5, it is also observed that, for D_2, the max-min scheme outperforms the Par scheme in terms of the SRT. Nevertheless, for the communication between S and D_1, the SRT of the max-min and Par schemes is the same. This observation confirms the fact that the outage and intercept probabilities of D_1 are not influenced by the max-min and Par schemes.

The SRT of the max-min and Par schemes for D_1 and D_2 with different power allocation coefficients α_1 and α_2 is described in Fig. 6. The first key observation is that, for D_2, the SRT of each relay selection scheme is improved as the power coefficient α_1 decreases from 0.2 to 0.1, and the improvement of the max-min scheme is more significant than that of the Par scheme. On the contrary, for D_1, when α_1 decreases from 0.2 to 0.1 as well, the SRT of both proposed relay selection

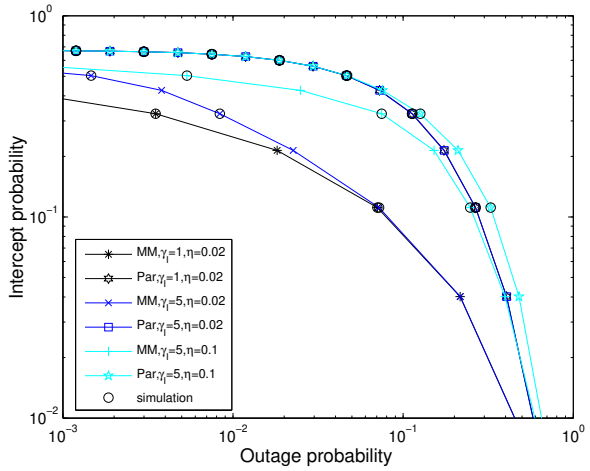

Fig. 7: The SRT of the max-min and Par relay selection schemes for D_2 with different γ_I and η when $\alpha_1 = 0.1$, $M = 6$, $\gamma_{o2} = 3$ and $\gamma_{e2} = 2$.

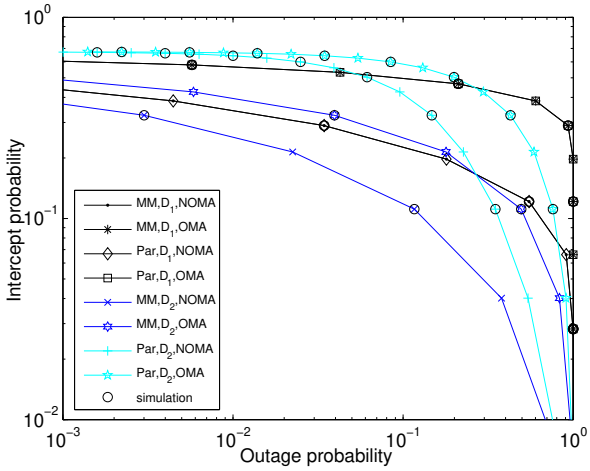

Fig. 8: The SRT of the max-min and Par relay selection for the NOMA and OMA schemes with $\alpha_1 = 0.1$, $N = 6$, $M = 6$, $r_{o2} = 1$, $r_{o1} = 2$ and $r_{o1} - r_{s1} = r_{o2} - r_{s2} = 0.8$.

schemes is degraded. Another important observation is that, for D_2, the SRT of the max-min scheme is better than that of the Par scheme when $\alpha_1 = 0.1$. However, in the case of $\alpha_1 = 0.2$, the Par scheme outperforms the max-min scheme in terms of SRT at low SNR, while the max-min scheme achieves a better SRT performance than the Par scheme in the moderate/high SNR regime. This indicates that the power allocation coefficient α_1 is a dominant factor that determines the SRT performance. In addition, it is worth noting that the max-min scheme has the same SRT performance as the Par scheme for a given α_1 for D_1.

The impact of γ_I and η on the SRT of the max-min and Par relay selection schemes for D_2 with $\alpha_1 = 0.1$ and $M = 6$ is presented in Fig. 7. It is observed that, when $\eta = 0.02$, the SRT of the max-min scheme is obviously degraded as the threshold γ_I increases from 1 to 5. However, the SRT of the Par scheme is almost unchanged with an increase of γ_I. In the case of $\gamma_I = 5$, it is noted that as the ratio η increases from 0.02 to 0.1, the SRT performance of each relay selection is significantly reduced. Furthermore, the degradation of SRT for the max-min scheme is more evident. The reason is that an increase of γ_I or η leads to an enhancement of RSI power.

In Fig. 8, we compare the SRT performance of the NOMA scheme with that of the OMA scheme for the max-min and Par relay selection. When the OMA scheme is employed, the data transmission from the source S to the users D_1 and D_2 requires three phases. It follows that the thresholds are $\gamma_{o1} = 2^{3r_{o1}} - 1$, $\gamma_{o2} = 2^{3r_{o2}} - 1$, $\gamma_{e1} = 2^{3(r_{o1} - r_{s1})} - 1$ and $\gamma_{e2} = 2^{3(r_{o2} - r_{s2})} - 1$ in the OMA-enabled two users cooperative network. According to the OMA scheme, two AN signals are transmitted, respectively, to confuse the eavesdropper as the source transmits messages x_1 and x_2. Thus, we assume that the transmit power of the AN signals in the cooperative OMA network is only half of the transmit power of the AN signal in the cooperative NOMA network. It can be observed from Fig. 8 that the NOMA scheme can achieve better SRT performance than that the OMA scheme for both max-min and Par relay selection at the users D_1 and D_2. It can also be seen that the SRT performance of the max-min selection scheme is better than that of the Par relay selection scheme for the far-user D_2 in the cooperative OMA network. However, for the OMA scheme, the max-min relay selection shows a similar SRT performance as that of the Par relay selection at the near-user D_1.

V. Conclusion

In this paper, we studied the PLS in the cooperative NOMA network, in which the source transmits messages to the multi-antenna near-user directly, and to the far-user with the help of multiple FD DF relays in the presence of an eavesdropper. The AN and relay selection techniques have been jointly designed to prevent information leakage in the considered wiretap communication system. Based on the closed-form expressions for the outage probability and intercept probability of the AN-aided max-min and Par relay selection schemes, we carried out the SRT performance analysis for the proposed relay selection schemes. Numerical results show that increasing the number of relays can improve the SRT of the max-min and Par schemes for D_2, and the improvement of the max-min scheme is much more evident than that of the Par scheme. However, the SRT of the near-user D_1 is not affected by the max-min and Par schemes. On the other hand, increasing the number of antennas can significantly enhance the SRT of D_1. Furthermore, when we decrease the power allocation coefficient α_1, the SRT of the max-min/Par scheme for D_2 is improved, but the SRT of each relay selection for D_1 is degraded. For the confidential data transmission from S to the far-user D_2, the max-min scheme outperforms the Par scheme in terms of SRT, and an increase of γ_I or η leads to a degradation of SRT for each relay selection scheme. Additionally, it is shown that although the eavesdropper can intercept the links from the source S to relays, it can not extract more information from the message for the far-user than for the near-user in the high SNR regime.

Thus, the proposed DF-XOR relaying protocol can effectively enhance the secrecy performance of the communication link between S and D_2. According to the obtained results, the performance of PLS in the design of practical communication systems (i.e., UAV communications and 5G and beyond wireless communications) can be enhanced by increasing the number of antennas and the relays, or adopting the max-min relay selection scheme and AN technique.

Besides the max-min and Par schemes, the two-stage relay selection will be investigated in our future work for the proposed wiretap multiple relays assisted cooperative NOMA network. Moreover, the considered wiretap system can be extended to a scenario with a multi-antenna eavesdropper or multiple eavesdroppers. In addition, investigating other secrecy performance metrics such as the secrecy outage probability, secrecy diversity order, secrecy rate and secrecy throughput of the AN-aided relay selection for the wiretap cooperative NOMA network is another promising future direction.

Appendix A
Proof for Theorem 1

The outage probability of the max-min scheme for D_1 is defined as follows:

$$\begin{aligned} P_{out1}^{\mathrm{I}} &= 1-\sum_{i=1}^{M}\Pr\{Z_i<\min\{|h_{si}|^2,|h_{id_2}|^2\}\} \\ &\quad \Pr\Big\{|\mathbf{w}^\dagger\mathbf{h}_{sd_1}|^2>\max\Big\{\frac{\gamma_{o1}\sigma_{d_1}^2}{\alpha_1 P_s},\frac{\gamma_{o2}\sigma_{d_1}^2 P_s^{-1}}{\alpha_2-\alpha_1\gamma_{o2}}\Big\}\Big\} \\ &= 1-\Pr\{|\mathbf{w}^\dagger\mathbf{h}_{sd_1}|^2>\max\{\gamma_{o1}\sigma_{d_1}^2[\alpha_1 P_s]^{-1}, \\ &\quad \gamma_{o2}\sigma_{d_1}^2[P_s(\alpha_2-\alpha_1\gamma_{o2})]^{-1}\}\} \\ &= 1-\int_{\max\left\{\frac{\gamma_{o1}\sigma_{d_1}^2}{\alpha_1 P_s},\frac{\gamma_{o2}\sigma_{d_1}^2 P_s^{-1}}{\alpha_2-\alpha_1\gamma_{o2}}\right\}}^{\infty}\frac{dx}{f^{-1}_{|\mathbf{w}^\dagger\mathbf{h}_{sd_1}|^2}(x)} \quad (A.1) \end{aligned}$$

where $Z_i = \max\limits_{j\in\mathcal{R}-\{i\}}\min\{|h_{sj}|^2,|h_{jd_2}|^2\}$. Substituting (5) into (A.1), P_{out1}^{I} can be written as (18).

Based on (14) and the total probability formula [31], [32], the intercept probability of the max-min scheme for D_1 is written as

$$P_{int1}^{\mathrm{I}}=\sum_{i=1}^{M}(Q_{1i}+Q_{2i})\Pr\{Z_i<\min\{|h_{si}|^2,|h_{id_2}|^2\}\}, \quad (A.2)$$

where $Q_{1i}=\Pr\{\Gamma_{ie1}^{[1]}>\gamma_{e1}\}$ and $Q_{2i}=\Pr\{\Gamma_{ie1}^{[1]}<\gamma_{e1},\Gamma_{ie1J}>\gamma_{e1},\frac{P_s|h_{se}|^2}{\sigma_e^2}>\gamma_{e1}\}$. Adopting the assumption that $|h_{sj}|^2$, $|h_{jd_2}|^2$ are independent exponential random variables, we compute the CDF of $\min\{|h_{si}|^2,|h_{id_2}|^2\}$ as follows:

$$\begin{aligned} F_{\min\{|h_{si}|^2,|h_{id_2}|^2\}}(x) &= 1-\Pr\{|h_{si}|^2>x,|h_{id_2}|^2>x\} \\ &= 1-e^{-(\lambda_{si}^{-1}+\lambda_{id_2}^{-1})x}. \quad (A.3) \end{aligned}$$

Owing to the assumption that the CSI of different links are statistically independent, we conclude that the random variables $\min\{|h_{s1}|^2,|h_{1d_2}|^2\},\cdots,\min\{|h_{sM}|^2,|h_{Md_2}|^2\}$ are independent of each other. Hence, applying (A.3) and the formula for multinomial expansion, the probability $\Pr\{Z_i<x\}$ is given by

$$\begin{aligned} \Pr\{Z_i<x\} &= \prod_{j\in\mathcal{R}-\{i\}}F_{\min\{|h_{sj}|^2,|h_{jd_2}|^2\}}(x) \\ &= \sum_{l=0}^{M-1}\sum_{\mathcal{A}\subset\mathcal{R}-\{i\},|\mathcal{A}|=l}(-1)^l e^{-x\sum\limits_{j\in\mathcal{A}}(\lambda_{sj}^{-1}+\lambda_{jd_2}^{-1})}. \quad (A.4) \end{aligned}$$

Utilizing (A.3) and (A.4), $\Pr\left\{Z_i<\min\{|h_{si}|^2,|h_{id_2}|^2\}\right\}$ can be defined as

$$\begin{aligned} &\Pr\{Z_i<\min\{|h_{si}|^2,|h_{id_2}|^2\}\} \\ &= \sum_{l=0}^{M-1}\sum_{\mathcal{A}\subset\mathcal{R}-\{i\},|\mathcal{A}|=l}\frac{(-1)^l}{1+\sum\limits_{j\in\mathcal{A}}\frac{\lambda_{sj}^{-1}+\lambda_{jd_2}^{-1}}{\lambda_{si}^{-1}+\lambda_{id_2}^{-1}}}. \quad (A.5) \end{aligned}$$

Furthermore, Q_{1i} in (A.2) is calculated as

$$\begin{aligned} Q_{1i} &= \int_0^{\infty}\Pr\{P_s|h_{se}|^2>\gamma_{e1}(P_1x+\sigma_e^2)\}f_{|h_{ie}|^2}(x)dx \\ &= \frac{\lambda_{se}P_s}{\lambda_{se}P_s+\lambda_{ie}P_1\gamma_{e1}}e^{-\frac{\gamma_{e1}\sigma_e^2}{\lambda_{se}P_s}}. \quad (A.6) \end{aligned}$$

The probability Q_{2i} for $\gamma_{e1}\geqslant 1$ and $0<\gamma_{e1}<1$ can be formulated, respectively, as

$$\begin{aligned} Q_{2i} &= \int_{\frac{\sigma_e^2\gamma_{e1}}{P_s}}^{\infty}\frac{f_{|h_{se}|^2}(x)dx}{\Pr\{P_1|h_{ie}|^2>P_s\gamma_{e1}x+\sigma_e^2\gamma_{e1}\}^{-1}} \quad (A.7) \\ Q_{2i} &= \int_{P_s^{-1}\sigma_e^2\gamma_{e1}}^{\frac{P_s^{-1}\sigma_e^2\gamma_{e1}}{1-\gamma_{e1}}}\frac{f_{|h_{se}|^2}(x)dx}{\Pr\{P_1|h_{ie}|^2>P_s\gamma_{e1}x+\gamma_{e1}^{-1}\sigma_e^2\}^{-1}} \\ &\quad +\int_{\frac{P_s^{-1}\sigma_e^2}{\gamma_{e1}^{-1}-1}}^{\infty}\frac{f_{|h_{se}|^2}(x)dx}{\Pr\{P_1|h_{ie}|^2>P_s\gamma_{e1}^{-1}x-\sigma_e^2\}^{-1}}. \quad (A.8) \end{aligned}$$

We can obtain closed-from expression of Q_{2i} as (20) by solving the integrals in (A.7) and (A.8). Finally, substituting Q_{1i},Q_{2i} and (A.5) into (A.2), the intercept probability P_{int1}^{I} can be derived.

Appendix B
Proof for Theorem 2

In the following, we assume that $\min\{P_s,P_1,P_2\}\to\infty$. For the SINR $\Gamma_{sd_1}^{[2]}$ in (3), we have

$$\begin{aligned} \lim_{P_s\to\infty}\Gamma_{sd_1}^{[2]} &= \lim_{P_s\to\infty}\frac{\alpha_2 P_s|\mathbf{w}^\dagger\mathbf{h}_{sd_1}|^2}{\alpha_1 P_s|\mathbf{w}^\dagger\mathbf{h}_{sd_1}|^2+\sigma_{d_1}^2} \\ &= \alpha_2\alpha_1^{-1}. \quad (B.1) \end{aligned}$$

Using the Remark 3 in [51], the outage probability P_{out1}^{I} is approximated as

$$\begin{aligned} P_{out1}^{\mathrm{I}} &\approx 1-\Pr\{|\mathbf{w}^\dagger\mathbf{h}_{sd_1}|^2>\gamma_{o1}\sigma_{d_1}^2(\alpha_1 P_s)^{-1}\} \\ &\approx [(N-1)!]^{-1}(\frac{\sigma_{d_1}^2\gamma_{o1}}{\lambda_{sd_1}P_s\alpha_1})^{N-1}. \quad (B.2) \end{aligned}$$

To derive the asymptotic expression for the intercept probability P_{int1}^{I}, it is required to derive the approximations of $\Pr\left\{Z_i<\min\{|h_{si}|^2,|h_{id_2}|^2\}\right\}$, Q_{1i} and Q_{2i}.

When $P\to\infty$, we can approximate the probability

$\Pr\{Z_i < \min\{|h_{si}|^2, |h_{id_2}|^2\}\}$ as follows:

$$\begin{aligned}
&\Pr\{Z_i < \min\{|h_{si}|^2, |h_{id_2}|^2\}\} \\
= \;& \Pr\{PZ_i < P\min\{|h_{si}|^2, |h_{id_2}|^2\}\} \\
\overset{(a)}{\approx} \;& \int_0^{P\beta_1} \frac{\big(\frac{1}{P\lambda_{si}} + \frac{1}{P\lambda_{id_2}}\big)\big(1-(\frac{1}{P\lambda_{si}} + \frac{1}{P\lambda_{id}})t\big)dt}{\big[\prod\limits_{j\in\mathcal{R}-\{i\}}\big(\frac{1}{P\lambda_{sj}} + \frac{1}{P\lambda_{jd_2}}\big)t\big]^{-1}} \\
\approx \;& \frac{\beta_1^M}{M}\big[\prod_{j\in\mathcal{R}}(\frac{1}{\lambda_{sj}} + \frac{1}{\lambda_{jd_2}})\big], \qquad \text{(B.3)}
\end{aligned}$$

where $\beta_1 = \min\limits_{j\in\mathcal{R}}(\frac{1}{\lambda_{sj}} + \frac{1}{\lambda_{jd_2}})^{-1}$, and the step (a) is obtained by the limit $\lim\limits_{P\to\infty} e^{-(\frac{1}{P\lambda_{sj}} + \frac{1}{P\lambda_{jd_2}})t} = 1-(\frac{1}{P\lambda_{sj}} + \frac{1}{P\lambda_{jd_2}})t$ and changing the integral region appropriately. Next, since $|h_{se}|^2$ and $|h_{ie}|^2$ are exponential random variables, the Q_{1i} and Q_{2i} can be approximated, respectively, as

$$\begin{aligned}
Q_{1i} &\approx \int_0^\infty \Pr\{P_s|h_{se}|^2 > P_1\gamma_{e1}x\} f_{|h_{ie}|^2}(x)dx \\
&= \frac{P_s\lambda_{se}}{P_s\lambda_{se} + P_1\lambda_{ie}\gamma_{e1}}, \qquad \text{(B.4)} \\
Q_{2i} &\approx \Pr\Big\{\frac{P_1|h_{ie}|^2}{P_s|h_{se}|^2} > \max\{\gamma_{e1}, \gamma_{e1}^{-1}\}, \frac{P_s|h_{se}|^2}{\sigma_e^2} > \gamma_{e1}\Big\} \\
&= \int_{\frac{\gamma_{e1}\sigma_e^2}{P_s}}^\infty \frac{f_{|h_{se}|^2}(x)dx}{\Pr\{|h_{ie}|^2 > \max\{\gamma_{e1}, \gamma_{e1}^{-1}\}P_1^{-1}P_s x\}^{-1}} \\
&\approx \frac{P_1\lambda_{ie}\min\{\gamma_{e1}, \gamma_{e1}^{-1}\}}{P_s\lambda_{se} + P_1\lambda_{ie}\min\{\gamma_{e1}, \gamma_{e1}^{-1}\}}. \qquad \text{(B.5)}
\end{aligned}$$

Finally, substituting (B.3)-(B.5) into (A.2), the approximation of P_{int1}^{I} can be expressed as (22).

Appendix C
Proof for Theorem 3

Employing the total probability formula [31], [32], the outage probability of the max-min scheme can be written as

$$P_{out2}^{\mathrm{I}} = 1 - \sum_{i=1}^{M}(P_{1i} + P_{2i}), \qquad \text{(C.1)}$$

where $P_{1i} = \Pr\{\Gamma_{si}^{[2]} > \gamma_{o2}, \Gamma_{id_2J} > \gamma_{o2}, \Gamma_{id_22} > \gamma_{o2}, |h_{si}|^2 > |h_{id_2}|^2 > Z_i\}$ and $P_{2i} = \Pr\{\Gamma_{si}^{[2]} > \gamma_{o2}, \Gamma_{id_2J} > \gamma_{o2}, \Gamma_{id_22} > \gamma_{o2}, |h_{id_2}|^2 > |h_{si}|^2 > Z_i\}$.

We denote $\theta_{1i} = \frac{\gamma_{o2}\sigma_i^2}{(\alpha_2 - \alpha_1\gamma_{o2})P_s}$ and $\theta_0 = \gamma_{o2}\max\{\frac{\sigma_{d_2}^2}{P_1}, \frac{\sigma_{d_2}^2}{P_2}\}$. The calculation of P_{1i} is divided into two categories: $\theta_0 \leqslant \theta_{1i}$ and $\theta_0 > \theta_{1i}$. Firstly, in the case of $\theta_0 \leqslant \theta_{1i}$, the term P_{1i} can be defined as

$$\begin{aligned}
P_{1i} &= \int_{\theta_0}^{\theta_{1i}}\int_{\theta_{1i}}^\infty \Pr\{\Gamma_{ii} < \theta_{1i}^{-1}t - 1\} f_{|h_{si}|^2}(t)dt \\
&\quad \times \Pr\{Z_i < x\} f_{|h_{id_2}|^2}(x)dx \\
&\quad + \int_{\theta_{1i}}^\infty\int_x^\infty \Pr\{\Gamma_{ii} < \theta_{1i}^{-1}t - 1\} f_{|h_{si}|^2}(t)dt \\
&\quad \times \Pr\{Z_i < x\} f_{|h_{id_2}|^2}(x)dx. \qquad \text{(C.2)}
\end{aligned}$$

According to (8), we can rewrite P_{1i} as

$$\begin{aligned}
P_{1i} &= \int_{\theta_0}^{\theta_{1i}}\Big[\int_{\theta_{1i}}^{\theta_{1i}(\gamma_I+1)} \Pr\{\Gamma_{ii} < \theta_{1i}^{-1}t - 1\} f_{|h_{si}|^2}(t)dt \\
&\quad + \int_{\theta_{1i}(\gamma_I+1)}^\infty f_{|h_{si}|^2}(t)dt\Big]\frac{f_{|h_{id_2}|^2}(x)dx}{\Pr\{Z_i < x\}^{-1}} \\
&\quad + \int_{\theta_{1i}}^{\theta_{1i}(\gamma_I+1)}\Big[\int_x^{\theta_{1i}(\gamma_I+1)} \Pr\{\Gamma_{ii} < \theta_{1i}^{-1}t - 1\} \\
&\quad \times f_{|h_{si}|^2}(t)dt + \int_{\theta_{1i}(\gamma_I+1)}^\infty f_{|h_{si}|^2}(t)dt\Big]\Pr\{Z_i < x\} \\
&\quad \times f_{|h_{id_2}|^2}(x)dx + \int_{\theta_{1i}(\gamma_I+1)}^\infty\int_x^\infty f_{|h_{si}|^2}(t)dt \\
&\quad \times \Pr\{Z_i < x\} f_{|h_{id_2}|^2}(x)dx. \qquad \text{(C.3)}
\end{aligned}$$

Computing the integral in (C.3), the probability P_{1i} is given in (25) where

$$\begin{aligned}
\delta_{1i\mathcal{A}} &= \lambda_{si}^{-1} + \lambda_{id_2}^{-1} + \sum_{j\in\mathcal{A}}(\lambda_{sj}^{-1} + \lambda_{jd_2}^{-1}), \\
\delta_{2i\mathcal{A}} &= \delta_{1i\mathcal{A}} + \sigma_i^2(P_1\lambda_{ii}\theta_{1i})^{-1}, \delta_{3i\mathcal{A}} = \delta_{1i\mathcal{A}} - \lambda_{si}^{-1}, \\
\eta_{1i} &= (1 - e^{-\sigma_i^2\gamma_I(P_1\lambda_{ii})^{-1}})^{-1}(e^{-\lambda_{si}^{-1}\theta_{1i}} \\
&\quad - \frac{P_1\lambda_{ii}\theta_{1i}e^{\sigma_i^2(P_1\lambda_{ii})^{-1} - (\lambda_{si}^{-1} + \sigma_i^2(P_1\lambda_{ii}\theta_{1i})^{-1})\theta_{1i}}}{P_1\lambda_{ii}\theta_{1i} + \lambda_{si}\sigma_i^2}), \\
\eta_{2i} &= \Big[\frac{e^{\frac{\sigma_i^2}{P_1\lambda_{ii}} - (\gamma_I+1)(\lambda_{si}^{-1} + \frac{\sigma_i^2}{P_1\lambda_{ii}\theta_{1i}})\theta_{1i}}}{(P_1\lambda_{ii}\theta_{1i})^{-1}(P_1\lambda_{ii}\theta_{1i} + \lambda_{si}\sigma_i^2)} - e^{-\frac{\gamma_I+1}{\lambda_{si}\theta_{1i}^{-1}}}\Big] \\
&\quad \times (1 - e^{-\sigma_i^2\gamma_I(P_1\lambda_{ii})^{-1}})^{-1} + e^{-(\gamma_I+1)\lambda_{si}^{-1}\theta_{1i}}.
\end{aligned}$$

On the other hand, when $\theta_0 > \theta_{1i}$, P_{1i} is expressed as

$$\begin{aligned}
P_{1i} &= \int_{\theta_0}^\infty\int_x^\infty \Pr\{\Gamma_{ii} < \theta_{1i}^{-1}t - 1\} f_{|h_{si}|^2}(t)dt \\
&\quad \times \Pr\{Z_i < x\} f_{|h_{id_2}|^2}(x)dx. \qquad \text{(C.4)}
\end{aligned}$$

Obviously, following the same steps as in the derivation of (25), P_{1i} can be obtained directly for $\theta_0 > \theta_{1i}$.

Taking into account the case of $\theta_0 \leqslant \theta_{1i}$, we can write P_{2i} as

$$\begin{aligned}
P_{2i} &= \int_{\theta_{1i}}^\infty \Pr\{\Gamma_{ii} < \theta_{1i}^{-1}|h_{si}|^2 - 1, x > |h_{si}|^2 > Z_i\} \\
&\quad \times f_{|h_{id_2}|^2}(x)dx \\
&= \int_{\theta_{1i}}^\infty\int_{\theta_{1i}}^x \Pr\{\Gamma_{ii} < \theta_{1i}^{-1}t - 1\}\Pr\{Z_i < t\} \\
&\quad \times f_{|h_{si}|^2}(t)dt f_{|h_{id_2}|^2}(x)dx. \qquad \text{(C.5)}
\end{aligned}$$

Similar to the derivation of (C.3), P_{2i} can be expressed as

$$\begin{aligned}
P_{2i} &= \int_{\theta_{1i}}^{\theta_{1i}(\gamma_I+1)}\int_{\theta_{1i}}^x \Pr\{\Gamma_{ii} < \theta_{1i}^{-1}t - 1\}\Pr\{Z_i < t\} \\
&\quad \times f_{|h_{si}|^2}(t)dt f_{|h_{id_2}|^2}(x)dx + \int_{\theta_{1i}(\gamma_I+1)}^\infty \\
&\quad \Big[\int_{\theta_{1i}}^{\theta_{1i}(\gamma_I+1)} \frac{\Pr\{Z_i < t\} f_{|h_{si}|^2}(t)dt}{\Pr\{\Gamma_{ii} < \theta_{1i}^{-1}t - 1\}^{-1}} \\
&\quad + \int_{\theta_{1i}(\gamma_I+1)}^x \frac{f_{|h_{si}|^2}(t)dt}{\Pr\{Z_i < t\}^{-1}}\Big] f_{|h_{id_2}|^2}(x)dx. \qquad \text{(C.6)}
\end{aligned}$$

Calculating the integral in (C.6), we can derive the closed-from expression of P_{2i} in (26) where

$$\begin{aligned}\eta_{3i} &= e^{-(\delta_{1i\mathcal{A}}-\lambda_{id_2}^{-1})\theta_{1i}}[(\delta_{1i\mathcal{A}}-\lambda_{id_2}^{-1})^{-1}-(\delta_{2i\mathcal{A}}-\lambda_{id_2}^{-1})^{-1}\\ &\quad\times e^{\sigma_i^2(P_1\lambda_{ii})^{-1}}],\\ \eta_{4i} &= [(e^{-(\delta_{1i\mathcal{A}}-\lambda_{id_2}^{-1})\theta_{1i}}-e^{-(\gamma_I+1)(\delta_{1i\mathcal{A}}-\lambda_{id_2}^{-1})\theta_{1i}})\\ &\quad\times(\delta_{1i\mathcal{A}}-\lambda_{id_2}^{-1})^{-1}-e^{\sigma_i^2(P_1\lambda_{ii})^{-1}}(e^{-(\delta_{2i\mathcal{A}}-\lambda_{id_2}^{-1})\theta_{1i}}\\ &\quad-e^{-(\gamma_I+1)(\delta_{2i\mathcal{A}}-\lambda_{id_2}^{-1})\theta_{1i}})(\delta_{2i\mathcal{A}}-\lambda_{id_2}^{-1})^{-1}]\\ &\quad\times(1-e^{-\frac{\sigma_i^2\gamma_I}{P_1\lambda_{ii}}})^{-1}+\frac{e^{-(\gamma_I+1)(\delta_{1i\mathcal{A}}-\lambda_{id_2}^{-1})\theta_{1i}}}{\delta_{1i\mathcal{A}}-\lambda_{id_2}^{-1}}.\end{aligned}$$

When $\theta_0 > \theta_{1i}$, P_{2i} can be presented as

$$\begin{aligned}P_{2i} &= \int_{\gamma_{o2}\max\left\{\frac{\sigma_{d_2}^2}{P_1},\frac{\sigma_{d_2}^2}{P_2}\right\}}^{\infty}\Pr\{\Gamma_{ii}<\theta_{1i}^{-1}|h_{si}|^2-1,\\ &\quad x>|h_{si}|^2>Z_i\}f_{|h_{id_2}|^2}(x)dx. \qquad \text{(C.7)}\end{aligned}$$

Consequently, adopting the same method previously used for deriving (26), we can define the closed-form expression of P_{2i} for $\theta_0 > \theta_{1i}$.

Therefore, when $\theta_0 \leqslant \theta_{1i}$, the closed-form expression of P_{out2}^{I} is evaluated as in (23).

With (16) and the total probability formula [31], [32], the intercept probability P_{int2}^{I} can be expressed as

$$\begin{aligned}P_{int2}^{\mathrm{I}} &= \sum_{i=1}^{M}\Pr\{Z_i<\min\{|h_{si}|^2,|h_{id_2}|^2\}\}\\ &\quad\times(\underbrace{\Pr\{\Gamma_{ie1}^{[2]}<\gamma_{e2},\Gamma_{ie1J}>\gamma_{e2},\Gamma_{ie2}>\gamma_{e2}\}}_{Q_{4i}}\\ &\quad+\underbrace{\Pr\{\Gamma_{ie1}^{[2]}>\gamma_{e2}\}}_{Q_{3i}}). \qquad \text{(C.8)}\end{aligned}$$

The probability Q_{3i} is calculated as $Q_{3i} = P_s\lambda_{se}(P_s\lambda_{se}+P_1\lambda_{ie}\gamma_{e2})^{-1}e^{-\frac{\gamma_{e2}\sigma_e^2}{P_s\lambda_{se}}}$. However, the computation of Q_{4i} are defined for two categories: $\gamma_{e2} \geqslant 1$ and $0 < \gamma_{e2} < 1$. For the case of $\gamma_{e2} \geqslant 1$, Q_{4i} can be expressed as

$$\begin{aligned}Q_{4i} &= \Pr\Big\{\frac{P_1|h_{ie}|^2}{P_s|h_{se}|^2+\sigma_e^2}>\gamma_{e2},P_2|h_{ie}|^2\sigma_e^{-2}>\gamma_{e2}\Big\}\\ &= \int_{\gamma_{e2}\max\left\{\frac{\sigma_e^2}{P_1},\frac{\sigma_e^2}{P_2}\right\}}^{\infty}\Pr\Big\{|h_{se}|^2<\frac{P_1t}{P_s\gamma_{e2}}-\frac{\sigma_e^2}{P_s}\Big\}\\ &\quad\times f_{|h_{ie}|^2}(t)dt\\ &= e^{-\frac{\gamma_{e2}}{\lambda_{ie}}\max\left\{\frac{\sigma_e^2}{P_1},\frac{\sigma_e^2}{P_2}\right\}}-\frac{P_s\lambda_{se}\gamma_{e2}}{P_1\lambda_{ie}+P_s\lambda_{se}\gamma_{e2}}\\ &\quad\times e^{\frac{\sigma_e^2}{P_s\lambda_{se}}-\left(\frac{1}{\lambda_{ie}}+\frac{P_1}{P_s\lambda_{se}\gamma_{e2}}\right)\gamma_{e2}\max\left\{\frac{\sigma_e^2}{P_1},\frac{\sigma_e^2}{P_2}\right\}}. \qquad \text{(C.9)}\end{aligned}$$

On the other hand, when $0 < \gamma_{e2} < 1$, Q_{4i} can be formulated as

$$\begin{aligned}Q_{4i} &= \Pr\{P_s|h_{se}|^2<\gamma_{e2}(P_1|h_{ie}|^2+\sigma_e^2),\\ &\quad P_s|h_{se}|^2>\sigma_e^2\gamma_{e2}(1-\gamma_{e2})^{-1},P_2|h_{ie}|^2>\sigma_e^2\gamma_{e2}\}\\ &\quad+\Pr\{P_1|h_{ie}|^2(P_s|h_{se}|^2+\sigma_e^2)^{-1}>\gamma_{e2},\\ &\quad\frac{P_s|h_{se}|^2\sigma_e^{-2}}{1-\gamma_{e2}}<\gamma_{e2},\frac{P_2|h_{ie}|^2}{\sigma_e^2}>\gamma_{e2}\}, \qquad \text{(C.10)}\end{aligned}$$

where the first and second terms on the right side of (C.10) are denoted by φ_{1i} and φ_{2i}, respectively.

By employing the basic probability theory, φ_{1i} is given by

$$\begin{aligned}\varphi_{1i} &= \int_{\gamma_{e2}\max\left\{\frac{\sigma_e^2}{P_2},\frac{\sigma_e^2}{P_1(1-\gamma_{e2})}\right\}}^{\infty}\Pr\Big\{\frac{P_s^{-1}\sigma_e^2\gamma_{e2}}{1-\gamma_{e2}}<|h_{se}|^2\\ &\quad<\frac{P_1t+\sigma_e^2}{P_s\gamma_{e2}^{-1}}\Big\}f_{|h_{ie}|^2}(t)dt. \qquad \text{(C.11)}\end{aligned}$$

By carrying out some mathematical manipulations, the φ_{1i} is written as (28).

Additionally, the calculation of φ_{2i} is divided into two cases as well. In the cases of $\frac{\sigma_e^2\gamma_{e2}}{P_2} < \frac{\sigma_e^2\gamma_{e2}}{P_1(1-\gamma_{e2})}$ and $\frac{\sigma_e^2\gamma_{e2}}{P_2} \geqslant \frac{\sigma_e^2\gamma_{e2}}{P_1(1-\gamma_{e2})}$, φ_{2i} can be written, respectively, as

$$\begin{aligned}\varphi_{2i} &= \int_{\gamma_{e2}\max\left\{\frac{\sigma_e^2}{P_1},\frac{\sigma_e^2}{P_2}\right\}}^{\frac{\sigma_e^2\gamma_{e2}}{P_1(1-\gamma_{e2})}}\Pr\Big\{|h_{se}|^2<\frac{1}{P_s}\Big(\frac{P_1}{\gamma_{e2}}t-\sigma_e^2\Big)\Big\}\\ &\quad\times f_{|h_{ie}|^2}(t)dt+\Pr\Big\{|h_{se}|^2<\frac{\sigma_e^2\gamma_{e2}}{P_s(1-\gamma_{e2})}\Big\}\\ &\quad\times\int_{\frac{\sigma_e^2\gamma_{e2}}{P_1(1-\gamma_{e2})}}^{\infty}f_{|h_{ie}|^2}(t)dt, \qquad \text{(C.12)}\\ \varphi_{2i} &= \Pr\Big\{|h_{se}|^2<\frac{\sigma_e^2\gamma_{e2}}{P_s(1-\gamma_{e2})}\Big\}\int_{\frac{\sigma_e^2\gamma_{e2}}{P_2}}^{\infty}f_{|h_{ie}|^2}(t)dt\\ &= \Big(1-e^{-\frac{\sigma_e^2\gamma_{e2}}{P_s\lambda_{se}(1-\gamma_{e2})}}\Big)e^{-\frac{\sigma_e^2\gamma_{e2}}{P_2\lambda_{ie}}}. \qquad \text{(C.13)}\end{aligned}$$

After some algebraic manipulations, φ_{2i} is evaluated as (29).

Consequently, substituting the closed-form expressions of φ_{1i} and φ_{2i} into (C.10), we can derive the Q_{4i} for $0 < \gamma_{e2} < 1$. Finally, substituting Q_{3i}, Q_{4i} and (A.5) into (C.8), the intercept probability P_{int2}^{I} can be obtained.

Appendix D
Proof for Theorem 4

From (7), (9), (12) and (15), the outage probability P_{out2}^{I} can be approximated as

$$\begin{aligned}P_{out2}^{\mathrm{I}} &= 1-\Pr\{\Gamma_{si^*}^{[2]}>\gamma_{o2},\Gamma_{i^*d_2J}>\gamma_{o2},\Gamma_{i^*d_22}>\gamma_{o2}\}\\ &\overset{(b)}{\approx} 1-\Pr\{|h_{si^*}|^2>(\gamma_I+1)\theta_{1i^*},\\ &\quad|h_{i^*d_2}|^2>\gamma_{o2}\sigma_{d_2}^2\max\{P_1^{-1},P_2^{-1}\}\}\\ &\overset{(c)}{\approx} 1-\Pr\{\frac{\min\{|h_{si^*}|^2,|h_{i^*d_2}|^2\}}{(\gamma_I+1)^{-1}}>\theta_{1i^*}\}\\ &= \Pr\{\max_{i\in\mathcal{R}}\min\{|h_{si}|^2,|h_{id_2}|^2\}<(\gamma_I+1)\theta_{1i^*}\}\\ &\approx \prod_{i\in\mathcal{R}}\Pr\{\frac{\min\{|h_{si}|^2,|h_{id_2}|^2\}}{(\gamma_I+1)^{-1}}<\theta_{1i}\}. \qquad \text{(D.1)}\end{aligned}$$

As $\min\{P_s,P_1,P_2\}\to\infty$, by applying (8), we have $\Gamma_{ii}=\gamma_I$, which leads to step (b). Then, replacing $\gamma_{o2}\sigma_{d_2}^2\max\{\frac{1}{P_1},\frac{1}{P_2}\}$

with $(\gamma_I+1)\theta_{1i^*}$ yields step (c).

Furthermore, applying the limit that $\lim_{P_s\to\infty} 1 - e^{-(\lambda_{si}^{-1}+\lambda_{id_2}^{-1})(\gamma_I+1)\theta_{1i}} = (\lambda_{si}^{-1}+\lambda_{id_2}^{-1})(\gamma_I+1)\theta_{1i}$ and the Monte-Carlo method [52]-[54], the approximation of P_{out2}^{I} can be calculated as

$$\begin{aligned} P_{out2}^{\mathrm{I}} &\approx \prod_{i\in\mathcal{R}}\Big[1-e^{-(\lambda_{si}^{-1}+\lambda_{id_2}^{-1})(\gamma_I+1)\theta_{1i}}\Big] \\ &\overset{(d)}{\approx} \xi_M \prod_{i\in\mathcal{R}}\Big[\frac{\gamma_I+1}{\lambda_{si}\theta_{1i}^{-1}}+\frac{\max\{P_1^{-1},P_2^{-1}\}}{\lambda_{id_2}\gamma_{o2}^{-1}\sigma_{d_2}^{-2}}\Big], \end{aligned} \tag{D.2}$$

where step (d) is obtained by replacing $\lambda_{id_2}^{-1}(\gamma_I+1)\theta_{1i^*}$ with $\lambda_{id_2}^{-1}\gamma_{o2}\sigma_{d_2}^2\max\{P_1^{-1},P_2^{-1}\}$ and the coefficient ξ_M is determined by the Monte-Carlo method. Furthermore, when $(\gamma_I+1)\theta_{1i^*}=\gamma_{o2}\sigma_{d_2}^2\max\{P_1^{-1},P_2^{-1}\}$, we have $\xi_M=1$.

Next, we focus on the asymptotic performance of the intercept probability P_{int2}^{I}. Since $|h_{se}|^2$ and $|h_{ie}|^2$ are independent exponential random variables, the approximated expressions of the Q_{3i} and Q_{4i} can be defined, respectively, as

$$\begin{aligned} Q_{3i} &\approx \Pr\{P_s|h_{se}|^2>\gamma_{e2}P_1|h_{ie}|^2\} \\ &= \frac{P_s\lambda_{se}}{P_s\lambda_{se}+P_1\lambda_{ie}\gamma_{e2}} \end{aligned} \tag{D.3}$$

$$\begin{aligned} Q_{4i} &\approx \Pr\Big\{\frac{P_1|h_{ie}|^2}{P_s|h_{se}|^2}>\gamma_{e2},\frac{P_s|h_{se}|^2}{P_1|h_{ie}|^2}<\gamma_{e2}, \\ &\quad \frac{P_2|h_{ie}|^2}{\sigma_e^2}>\gamma_{e2}\Big\} \\ &= \int_{\frac{\sigma_e^2\gamma_{e2}}{P_2}}^{\infty}\Pr\Big\{|h_{se}|^2<\frac{\min\{\gamma_{e2},\gamma_{e2}^{-1}\}t}{P_sP_1^{-1}}\Big\}f_{|h_{ie}|^2}(t)dt \\ &\approx \frac{P_1\lambda_{ie}\min\{\gamma_{e2},\gamma_{e2}^{-1}\}}{P_1\lambda_{ie}\min\{\gamma_{e2},\gamma_{e2}^{-1}\}+P_s\lambda_{se}}. \end{aligned} \tag{D.4}$$

Finally, plugging (D.3), (D.4) and (B.3) into (C.8), the intercept probability P_{int2}^{I} can be defined approximately by

$$\begin{aligned} P_{int2}^{\mathrm{I}} &\approx \sum_{i=1}^{M}\frac{\beta_1^M}{M}\Big[\frac{P_1\lambda_{ie}\min\{\gamma_{e2},\gamma_{e2}^{-1}\}}{P_1\lambda_{ie}\min\{\gamma_{e2},\gamma_{e2}^{-1}\}+P_s\lambda_{se}} \\ &\quad +\frac{P_s\lambda_{se}}{P_s\lambda_{se}+P_1\lambda_{ie}\gamma_{e2}}\Big]\Big[\prod_{j\in\mathcal{R}}(\frac{1}{\lambda_{sj}}+\frac{1}{\lambda_{jd_2}})\Big] \end{aligned} \tag{D.5}$$

REFERENCES

[1] S. Pattar, R. Buyya, K. R. Venugopal, S. S. Iyengar, and L. M. Patnaik, "Searching for the IoT resources: Fundamentals, requirements, comprehensive review, and future directions," *IEEE Commun. Surv. Tut.*, vol. 20, no. 3, pp. 2101-2132, Jul. 2018.

[2] M. R. Palattella, M. Dohler, A. Grieco, G. Rizzo, J. Torsner, T. Engel, and L. Ladid, "Internet of Things in the 5G era: Enablers, architecture, and business models," *IEEE J. Sel. Areas Commun.*, vol. 34, no. 3, pp. 510-527, Mar. 2016.

[3] L. Chettri and R. Bera, "A comprehensive survey on Internet of Things (IoT) towards 5G wireless systems," *IEEE Internet Things J.*, vol. 7, no. 1, pp. 16-32, Jan. 2020.

[4] S. Lai, R. Zhao, S. Tang, J. Xia, L. Fan, "Intelligent secure mobile edge computing for beyond 5G wireless networks," *Physical Commun.*, vol. 45, no. 9, 101283, pp.1-8, Mar. 2021.

[5] P. Xu and K. Cumanan, "Optimal power allocation scheme for non-orthogonal multiple access with α-fairness," *IEEE J. Sel. Areas Commun.*, vol. 35, no. 10, pp. 2357-2369, Oct. 2017.

[6] F. Alavi, K. Cumanan, Z. Ding, and A. G. Burr, "Beamforming techniques for nonorthogonal multiple access in 5G cellular networks," *IEEE Trans. Veh. Technol.*, vol. 67, no. 10, pp. 9474-9487, Oct. 2018.

[7] F. Alavi, K. Cumanan, M. Fozooni, Z. Ding, S. Lambotharan and O. A. Dobre, "Robust energy-efficient design for MISO non-orthogonal multiple access systems," *IEEE Trans. Commun.*, vol. 67, no. 11, pp. 7937-7949, Nov. 2019.

[8] H. M. Al-Obiedollah, K. Cumanan, J. Thiyaglingam, J. Tang, A. G. Burr Z. Ding and O. A. Dobre, "Spectral-energy efficiency trade-off-based beamforming design for MISO non-orthogonal multiple access systems," *IEEE Trans. Wireless Commun.*, vol. 19, no. 10, pp. 6593-6606, Oct. 2020.

[9] S. Chen and J. Zhao, "The requirements, challenges, and technologies for 5G of terrestrial mobile telecommunication," *IEEE Commun. Mag.*, vol. 52, no.5, pp. 36-43, May 2014.

[10] M. Sami, N. K. Noordin, M. Khabazian, F. Hashim, and S. Subramaniam, "A survey and taxonomy on medium access control strategies for cooperative communication in wireless networks: Research issues and challenges," *IEEE Commun. Surveys Tuts.*, vol. 18, no. 4, pp. 2493-2521, Nov. 2016.

[11] M. Alkhawatrah, Y. Gong, G. Chen, S. Lambotharan, and J. A. Chambers, "Buffer-aided relay selection for cooperative NOMA in the Internet of Things," *IEEE Internet Things J.*, vol. 6, no. 3, pp. 5722-5731, Jun. 2019.

[12] X. Chen, G. Liu, Z. Ma, X. Zhang, W. Xu, and P. Fan, "Optimal power allocations for non-orthogonal multiple access over 5G full/half-duplex relaying mobile wireless networks," *IEEE Trans. Wireless Commun.*, vol. 18, no. 1, pp. 77-92, Jan. 2019.

[13] M. Zeng, W. Hao, O. A Dobre, and Z. Ding, "Cooperative NOMA: state of the art, key techniques, and open challenges," *IEEE Network*, vol. 34, issue 5, pp. 205-211, Jul. 2020.

[14] K. Cumanan, Z. Ding, B. Sharif, G. Y. Tian, and K. K. Leung, "Secrecy rate optimizations for a MIMO secrecy channel with a multiple-antenna Eavesdropper," *IEEE Trans. Veh. Technol.*, vol. 63, no. 4, pp. 1678-1690, May 2014.

[15] K. Cumanan, G. C. Alexandropoulos, Z. Ding, and G. K. Karagiannidis, "Secure communications with cooperative jamming: Optimal power allocation and secrecy outage analysis," *IEEE Trans. Veh. Technol.*, vol. 66, no. 8, pp. 7495-7505, Aug. 2017.

[16] K. Cumanan, H. Xing, P. Xu, G. Zheng, X. Dai, A. Nallanathan, Z. Ding, and G. Kargiannidis, "Physical layer security jamming: Theoretical limits and practical designs in wireless networks" *IEEE Access*, pp. 3603-3611, vol. 5, 2017.

[17] W. Wang, X. Li, M. Zhang, K. Cumanan, D. W. Kwan Ng, G. Zhang, J. Tang, and O. A. Dobre, "Energy-constrained UAV-assisted secure communications with position optimization and cooperative jamming," *IEEE Trans. Commun.*, vol. 68, no. 7, pp. 4476-4489, Jul. 2020.

[18] W. Wang, X. Li, R. Wang, K. Cumanan, W. Feng, Z. Ding and O. A. Dobre, "Robust 3D-trajectory and time switching optimization for dual-UAV-enabled secure communications," *IEEE J. Sel. Areas Commun.*, vol. 39, no. 11, pp. 3334-3347, Nov. 2021.

[19] X. Yue, Y. Liu, Y. Yao, X. Li, R. Liu and A. Nallanathan, "Secure communications in a unified non-orthogonal multiple access framework," *IEEE Trans. Wireless Commun.*, vol. 19, no. 3, pp. 2163-2178, Mar. 2020.

[20] C. Gong, X. Yue, Z. Zhang, X. Wang and X. Dai, "Enhancing physical layer security with artificial noise in large-scale NOMA networks," *IEEE Trans. Veh. Technol.*, vol. 70, no. 3, pp. 2349-2361, Mar. 2021,

[21] Z. Ding, Z. Zhao, M. Peng, and H. V. Poor, "On the spectral efficiency and security enhancements of NOMA assisted multicast-unicast streaming," *IEEE Trans. Commun.*, vol. 65, no. 7, pp. 3151-3163, Jul. 2017.

[22] F. Zhou, Z. Chu, H. Sun, R. Q. Hu, and L. Hanzo, "Artificial noise aided secure cognitive beamforming for cooperative MISO-NOMA using SWIPT," *IEEE J. Sel. Areas Commun.*, vol. 36, no. 4, pp. 918-931, April 2018.

[23] H.-M. Wang, X. Zhang, Q. Yang, and T. A. Tsiftsis, "Secure users oriented downlink MISO NOMA," *IEEE J. Sel. Topics Signal Process.*, vol. 13, no. 3, pp. 671-684, Jun. 2019.

[24] M. Zeng, N. Nguyen, O. A. Dobre, and H. V. Poor, "Securing downlink massive MIMO-NOMA networks with artificial noise," *IEEE J. Sel. Topics Signal Process.*, vol. 13, no. 3, pp. 685-699, June 2019.

[25] N.-P. Nguyen, M. Zeng, O. A. Dobre, and H. V. Poor, "Securing massive MIMO-NOMA networks with ZF beamforming and artificial noise," in *Proc. IEEE Global Communications Conference (GLOBECOM)*, Waikoloa, HI, USA, Dec. 2019, pp.1-6.

[26] D. Tran, H. Tran, D. Ha, and G. Kaddoum, "Secure transmit antenna selection protocol for MIMO NOMA networks over nakagami-m channels," *IEEE Syst. J.*, vol. 14, no. 1, pp. 253-264, Mar. 2020.

[27] J. Chen, L. Yang, and M.-S. Alouini, "Physical layer security for cooperative NOMA systems," *IEEE Trans. Veh. Technol.*, vol. 67, no. 5, pp. 4645-4649, May 2018.

[28] W. Xie, J. Liao, C. Yu, P. Zhu, and X. Liu, "Physical layer security performance analysis of the FD-based NOMA-VC system," *IEEE Access*, vol. 7, pp. 115568-115573, Aug. 2019.

[29] Z. Xiang, W. Yang, G. Pan, Y. Cai, and X. Sun, "Secure transmission in non-orthogonal multiple access networks with an untrusted relay," *IEEE Wireless Commun. Lett.*, vol. 8, no. 3, pp. 905-908, Jun. 2019.

[30] A. Arafa, W. Shin, M. Vaezi, and H. V. Poor, "Secure relaying in non-orthogonal multiple access: Trusted and untrusted scenarios," *IEEE Trans. Inf. Forensics Security*, vol. 15, no. 1, pp. 210-222, Jan. 2020.

[31] Y. Zou, B. Champagne, W.-P. Zhu, L. Hanzo, "Relay-selection improves the security-reliability trade-off in cognitive radio systems," *IEEE Trans. Commun.*, vol. 63, no. 1, pp. 215-228, Jan. 2015.

[32] X. Ding, Y. Zou, F. Ding, D. Zhang, and G. Zhang, "Opportunistic relaying against eavesdropping for Internet-of-Things: A security-reliability tradeoff perspective," *IEEE Internet Things J.*, vol. 6, no. 5, pp. 8727-8738, Oct. 2019.

[33] Y. Feng, S. Yan, C. Liu, Z. Yang, and N. Yang, "Two-stage relay selection for enhancing physical layer security in non-orthogonal multiple access," *IEEE Trans. Inf. Forensics Security*, vol. 14, no. 6, pp. 1670-1683, Jun. 2019.

[34] Z. Wang and Z. Peng, "Secrecy performance analysis of relay selection in cooperative NOMA systems," *IEEE Access*, vol. 7, pp. 86274-86287, Jul. 2019.

[35] C. Yu, H.-L. Ko, X. Peng, and W. Xie, "Secrecy outage performance analysis for cooperative NOMA over nakagami-m channel," *IEEE Access*, vol. 7, pp. 79866-79876, Jul. 2019.

[36] H. Lei, Z. Yang, K.-H. Park, I. S. Ansari, Y. Guo, G. Pan, and M. Alouini, "Secrecy outage analysis for cooperative NOMA systems with relay selection schemes," *IEEE Trans. Commun.*, vol. 67, no. 9, pp. 6282-6298, Sept. 2019.

[37] C. Yu, H.-L. Ko, X. Peng, W. Xie, and P. Zhu, "Jammer-aided secure communications for cooperative NOMA systems," *IEEE Commun. Lett.*, vol. 23, no. 11, pp. 1935-1939, Nov. 2019.

[38] Y. Cao, N. Zhao, G. Pan, Y. Chen, L. Fan, M. Jin, and M.-S. Alouini, "Secrecy analysis for cooperative NOMA networks with multi-antenna full-duplex relay," *IEEE Trans. Commun.*, vol. 67, no. 8, pp. 5574-5587, Aug. 2019.

[39] L. Lv, H. Jiang, Z. Ding, L. Yang, and J. Chen, "Secrecy-enhancing design for cooperative downlink and uplink NOMA with an untrusted relay," *IEEE Trans. Commun.*, vol. 68, no. 3, pp. 1698-1715, Mar. 2020.

[40] M. Yang, J. Chen, L. Yang, L. Lv, B. He and B. Liu, "Design and performance analysis of cooperative NOMA with coordinated direct and relay transmission," *IEEE Access*, vol. 7, pp. 73306-73323, Jun. 2019.

[41] Z. Yu, C. Zhai, J. Liu and H. Xu, "Cooperative relaying based non-orthogonal multiple access (NOMA) with relay selection," *IEEE Trans. Veh. Technol.*, vol. 67, no. 12, pp. 11606-11618, Dec. 2018.

[42] X. Shao, C. Yang, Y. Song, T. Li and Z. Han, "Game theoretical approaches for cooperative UAV NOMA networks," *IEEE Wireless Commun.*, vol. 28, no. 2, pp. 96-105, Apr. 2021.

[43] X. Jiang, Z. Wu, Z. Yin, Z. Yang and N. Zhao, "Power consumption minimization of UAV relay in NOMA networks," *IEEE Wireless Commun. Lett.*, vol. 9, no. 5, pp. 666-670, May 2020

[44] J. Katz and Y. Lindell, *Introduction to Modern Cryptography*, 2th ed. Boca Raton, USA: Chapman and Hall/CRC, 2015.

[45] G. Chen, Y. Gong, P. Xiao, and J. A. Chambers, "Physical layer network security in the full-duplex relay system," *IEEE Trans. Inf. Forensics Security*, vol. 10, no. 3, pp. 574-583, Mar. 2015.

[46] N. H. Mahmood, I. S. Ansari, P. Popovski, P. Mogensen, and K. A. Qaraqe, "Physical-layer security with full-duplex transceivers and multiuser receiver at Eve," *IEEE Trans. Commun.*, vol. 65, no. 10, pp. 4392-4405, Oct. 2017.

[47] T. Zhang, Y. Huang, Y. Cai, C. Zhong, W. Yang, and G. K. Karagiannidis, "Secure multi-antenna cognitive wiretap networks," *IEEE Trans. Veh. Technol.*, vol. 66, no. 5, pp. 4059-4072, May 2017.

[48] Y. Zou, "Physical-layer security for spectrum sharing systems," *IEEE Trans. Wireless Commun.*, vol. 16, no. 2, pp. 1319-1329, Feb. 2017.

[49] M. Mohammadi, X. Shi, B. K. Chalise, Z. Ding, H. A. Suraweera, C. Zhong, and J. S. Thompson, "Full-duplex non-orthogonal multiple access for next generation wireless systems," *IEEE Commun. Mag.*, vol. 57, no. 5, pp. 110-116, May 2019.

[50] M. Vaezi, R. Schober, Z. Ding and H. V. Poor, "Non-orthogonal multiple access: Common myths and critical questions," *IEEE Wireless Commun.*, vol. 26, no. 5, pp. 174-180, Oct. 2019.

[51] Z. Cao, X. Ji, J. Wang, S. Zhang, Y. Ji, and J. Wang, "Security-reliability tradeoff analysis for underlay cognitive two-way relay networks," *IEEE Trans. Wireless Commun.*, vol. 18, no. 12, pp. 6030-6042, Dec. 2019.

[52] H. Zhu and J. Wang, "Chunk-based resource allocation in OFDMA systems-Part I: Chunk allocation," *IEEE Trans. Commun.*, vol. 57, no. 9, pp. 2734-2744, Sep. 2009.

[53] H. Zhu and J. Wang, "Chunk-based resource allocation in OFDMA systems-Part II: Joint chunk, power and bit allocation," *IEEE Trans. Commun.*, vol. 60, no. 2, pp. 499-509, Feb. 2012.

[54] H. Zhu, "Radio resource allocation for OFDMA systems in high speed environments," *IEEE J. Sel. Areas Commun.*, vol. 30, no. 4, pp. 748-759, May 2012.

Zhanghua Cao received the B.S. and Ph.D. degrees in Applied Mathematics from Yangzhou University, Yangzhou, China, in 2005 and 2010, respectively. He is currently a Lecturer at the School of Information Science and Technology, Nantong University. His current research interests include cooperative relaying, nonorthogonal multiple access (NOMA), unmanned aerial vehicle communications and physical-layer security.

Xiaodong Ji (Member, IEEE) received the B.S. degree (with excellence) in electronic and information engineering from Nantong Institute of Technology, Nantong, China, in 2003, and the M.S. and Ph.D. degrees both in signal and information processing from Nanjing University of Posts and Telecommunications, Nanjing, China, in 2006 and 2012, respectively. He is currently an Associate Professor at the School of Information Science and Technology, Nantong University. From 2006 to 2009, he was a Lecturer with the School of Electronics and Information, Nantong University. From 2013 to 2015, he was a Post-Doctoral Fellow at the Department of Electrical and Computer Engineering, Concordia University, Montreal, Canada. His current research interests include cooperative relaying, physical-layer security, and cognitive radio technologies.

Jue Wang (Member, IEEE) received the B.S. degree in communications engineering from Nanjing University, Nanjing, China, in 2006, and the M.S. and Ph.D. degrees from the National Communications Research Laboratory, Southeast University, Nanjing, China, in 2009 and 2014, respectively. From 2014 to 2016, he was with the Singapore University of Technology and Design as a Post-Doctoral Research Fellow. He is currently with the School of Information Science and Technology, Nantong University, Nantong, China. His research interests include MIMO wireless communications, multiuser transmission, MIMO channel modeling, massive MIMO systems, and physical layer security. He has served as a Technical Program Committee Member for a number of IEEE conferences, and reviewer for various IEEE journals. He was awarded as an Exemplary Reviewer of the IEEE TRANSACTIONS ON COMMUNICATIONS in 2014.

Wei Wang (Member, IEEE) received the Ph.D. degree in communication and information system from Shanghai University, Shanghai, China, in 2011. He is currently an Associate Professor with the School of Information Science and Technology, Nantong University. He is also with the Peng Cheng Laboratory and the Nantong Research Institute for Advanced Communication Technologies. From Feb. 2016 to Aug. 2016, he was a Visiting Scholar in the Department of Electrical and Computer Engineering at the Boise State University, ID, USA. From Feb. 2019 to Aug. 2019, he was an Academic Visitor in the Department of Electronic Engineering at the University of York, York, UK. His current research interests include unmanned aerial vehicle communications, maritime communications, physical layer security, and machine learning for wireless communications.

Kanapathippillai Cumanan (Senior Member, IEEE) received the BSc degree with first class honors in electrical and electronic engineering from the University of Peradeniya, Sri Lanka in 2006 and the PhD degree in signal processing for wireless communications from Loughborough University, Loughborough, UK, in 2009.

He is currently a Senior Lecturer with the Department of Electronic Engineering, University of York, York, UK. From March 2012 to November 2014, he was working as a research associate at School of Electrical and Electronic Engineering, Newcastle University, UK. Prior to this, he was with the School of Electronic, Electrical and System Engineering, Loughborough University, UK. In 2011, he was an academic visitor at Department of Electrical and Computer Engineering, National University of Singapore, Singapore. From January 2006 to August 2006, he was an assistant lecturer with Department of Electrical and Electronic Engineering, University of Peradeniya, Sri Lanka. His research interests include non-orthogonal multiple access (NOMA), cell-free massive MIMO, physical layer security, cognitive radio networks, convex optimization techniques and resource allocation techniques. He has published more than 100 journal articles and conference papers which attracted more than 2300 Google scholar citations. He is currently an Associate Editor of the IEEE OPEN JOURNAL OF THE COMMUNICATIONS SOCIETY and IEEE ACCESS, and an Editor of the IEEE WIRELESS COMMUNICATIONS LETTERS.

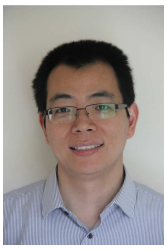

Zhiguo Ding (Fellow, IEEE) received his B.Eng in Electrical Engineering from the Beijing University of Posts and Telecommunications in 2000, and the Ph.D degree in Electrical Engineering from Imperial College London in 2005. From Jul. 2005 to Apr. 2018, he was working in Queen's University Belfast, Imperial College, Newcastle University and Lancaster University. Since Apr. 2018, he has been with the University of Manchester as a Professor in Communications. From Oct. 2012 to Sept. 2021, he has also been an Academic Visitor in Princeton University.

Dr Ding' research interests are 5G networks, game theory, cooperative and energy harvesting networks and statistical signal processing. He is serving as an Area Editor for the IEEE OPEN JOURNAL OF THE COMMUNICATIONS SOCIETY, an Editor for IEEE TRANSACTIONS ON VEHICULAR TECHNOLOGY, and JOURNAL OF WIRELESS COMMUNICATIONS AND MOBILE COMPUTING, and was an Editor for IEEE WIRELESS COMMUNICATION LETTERS, IEEE TRANSACTIONS ON COMMUNICATIONS, IEEE COMMUNICATION LETTERS from 2013 to 2016. He recently received the EU Marie Curie Fellowship 2012-2014, the Top IEEE TVT Editor 2017, IEEE Heinrich Hertz Award 2018, IEEE Jack Neubauer Memorial Award 2018, IEEE Best Signal Processing Letter Award 2018, and Friedrich Wilhelm Bessel Research Award 2020. He is a Fellow of the IEEE, a Distinguished Lecturer of IEEE ComSoc, and a Web of Science Highly Cited Researcher in two categories 2020.

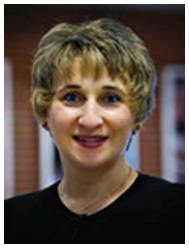

Octavia A. Dobre (Fellow, IEEE) received the Dipl. Ing. and Ph.D. degrees from the Polytechnic Institute of Bucharest, Romania, in 1991 and 2000, respectively. Between 2002 and 2005, she was with New Jersey Institute of Technology, USA. In 2005, she joined Memorial University, Canada, where she is currently a Professor and Research Chair. She was a Visiting Professor with Massachusetts Institute of Technology, USA and Université de Bretagne Occidentale, France. Her research interests encompass various wireless technologies, such as non-orthogonal multiple access and full duplex, as well as optical and underwater communications, and machine learning for communications. She has (co-)authored over 350 refereed papers in these areas.

Dr. Dobre serves as the Editor-in-Chief (EiC) of the IEEE OPEN JOURNAL OF THE COMMUNICATIONS SOCIETY. She was the EiC of the IEEE COMMUNICATIONS LETTERS, Senior Editor, Editor, and Guest Editor for various prestigious journals and magazines. She also served as General Chair, Technical Program Co-Chair, Tutorial Co-Chair, and Technical Co-Chair of symposia at numerous conferences.

Dr. Dobre was a Fulbright Scholar, Royal Society Scholar, and Distinguished Lecturer of the IEEE Communications Society. She obtained Best Paper Awards at various conferences, including IEEE ICC, IEEE Globecom, IEEE WCNC, and IEEE PIMRC. Dr. Dobre is a Fellow of the Engineering Institute of Canada.